

Multilongitudinal mode emission in ring cavity class B lasers

Eugenio Roldán, Germán J. de Valcárcel,
Departament d'Òptica, Universitat de València,
Dr. Moliner 50, 46100–Burjassot, Spain

Franco Prati
Istituto Nazionale per la Fisica della Materia, and
Dipartimento di Fisica e Matematica, Università dell'Insubria,
via Valleggio 11, I–22100 Como, Italy,

Fedor Mitschke, and Tom Voigt
Fachbereich Physik, Universität Rostock,
18051 Rostock, Germany

November 6, 2018

Abstract

In this article we review recent theoretical and experimental developments on multilongitudinal-mode emission in ring cavity lasers, paying special attention to class B lasers. We consider both homogeneously and inhomogeneously broadened amplifying media as well as the limits of small and large cavity losses (*i.e.*, we treat cases within and outside the uniform field limit approximation). In particular we discuss up to what extent the experimental observations of self-mode locking in erbium-doped fiber lasers carried out in recent years are a manifestation of the Risken-Nummedal-Graham-Haken instability.

1 INTRODUCTION: WHY SHOULD WE CARE ABOUT LASER INSTABILITIES?

The very first laser – Maiman's ruby in 1961 – produced extremely unstable emission, as evidenced by a figure in the original publication [1]. Soon thereafter, researchers began to learn the skills of how to avoid instabilities in lasers designed for applications. Nonetheless laser instabilities have been around ever since both as a nuisance lurking to haunt technically-minded people, and as an

interesting nontrivial physical phenomenon for the more fundamental-principles-minded set. After all, lasers are nonlinear dynamical feedback systems, and instabilities are inherent in such systems. It is certainly warranted to gain an understanding of laser instabilities – if only for the minimalist purpose that they be avoided successfully in spite of the ever increasing demands on lasers in terms of power, speed, tunability, etc.

In lasers, typically one or several modes of the light field are subject to resonator boundary conditions while at the same time being dynamically coupled to the amplifying medium. Typically the coupling is highly nonlinear, and depending on the laser type and particular circumstances, the laser may behave in many different ways, running the gamut from smooth and stable single-mode to irregular and unpredictable chaotic operation.

To systematically address the plethora of possibilities, one can make a first distinction between cases in which either several transverse modes are involved, or just a single one (TEM_{00}). Next-neighbor longitudinal modes always have very nearly the same frequency difference, and only a single beat frequency, along with its overtones, can occur. In contrast, for transverse modes there can be more beat frequencies, giving rise to an enormous wealth of possibilities for frequency locking and pulling phenomena. Maiman's ruby laser, for example, displayed an instability that involved several transverse modes. The complexity of the situation is not helped by the fact that a mathematical description requires either an infinite set of ordinary differential equations, or a set of fully space-dependent partial differential equations. Nonetheless, quite some research was devoted to multi-transverse mode dynamics (see [2, 3, 4] for references, and the rest of articles appearing in the present volume). More attention, however, was given to single mode laser instabilities over the last three decades. Overviews and references can be found, e.g., in [2, 3, 5, 6, 7, 8, 9, 10, 11, 12, 13].

Here we shall consider single-transverse mode problems. In this context, there is an important distinction whether several longitudinal cavity modes are involved in the lasing process, or just a single one, although a connection between singlemode and multimode instabilities can be established [14]. It is also of fundamental importance whether the gain medium exhibits a homogeneously or inhomogeneously broadened lasing transition (see, e.g., [2, 9]).

It was noticed by Haken in 1975 [15] that the Maxwell-Bloch model for a homogeneously broadened single mode laser is isomorphic to the Lorenz model of chaos, originally developed for climatic instability [16]. This directly implies that these lasers must exhibit a second threshold, *i.e.* a characteristic value of the pump power above which a Lorenz-type instability sets on. One can show that this second threshold is at least nine times higher than the first (ordinary) threshold above which there is coherent oscillation (see, e.g., [2, 9, 10, 15, 16]). This “factor-of-nine” is of great importance to the present paper. Later Weiss found [17] that certain far-infrared lasers have suitable damping rates and can be pumped hard enough to test this prediction. Indeed they displayed chaotic behavior remarkably similar in many respects to that exhibited by the Lorenz model [18, 19]. Unfortunately the level structure of the gain atoms was much more complex than a two-level system. The relevance of this difference for

the laser dynamics was the focus of some controversy during the eighties and the beginning of the nineties (see [20, 21] for a discussion at depth and for references). However, in the absence of a formal proof of equivalence between the realistic laser model and the Lorenz model, one can only cautiously conclude that some lasers can display Lorenz chaos even when their structure does not make it obvious that the Lorenz equations are the appropriate model.

In contrast, multilongitudinal mode laser emission has received only marginal attention from the viewpoint of laser instabilities. This is all the more remarkable considering that most lasers emit in several longitudinal modes, if only due to spectral hole burning in inhomogeneously broadened active media (see, e.g., [22, 23, 24]).

It is a common belief that with a homogeneously broadened gain line and single-transverse mode condition, the only way to have more than one longitudinal mode oscillating is spatial inhomogeneity in the medium, such as the spatial hole burning occurring in linear resonators. The spatial inhomogeneity provides the required amount of independence of the inversion available to one mode from that available to another mode so that the usual winner-takes-all coupling is suspended in favor of the mild mutual coupling due the finite overall energy balance¹.

This myth was shattered when in 1968 two publications, independent of each other, discussed the situation in detail [29, 30] (see also [31]). It was shown that even in a unidirectional resonator filled with a perfectly homogeneous medium, Rabi splitting of the lasing transition induced by the lasing mode can provide gain for other longitudinal modes. This means that even perfect gain homogeneity does not safeguard against instability. While a string of four names makes a somewhat awkward moniker, fairness dictates to call this mechanism the *Risken-Nummedal-Graham-Haken Instability*, or RNGHI for short. Ikeda *et al.* introduced the term *Resonant Rabi Instability* for designating this instability [32]².

In [29, 30, 31] a unidirectional ring cavity with small cavity losses filled with a homogeneously broadened two-level active medium was assumed. The prediction was that for RNGHI to occur the pump power must exceed a certain instability threshold. This instability threshold is referred to as the *second threshold*, in distinction to the familiar first threshold which defines the onset of coherent laser oscillation. The value of the second threshold came out to be

¹A good deal of theoretical and experimental work has been done in order to correctly understand multimode emission in Fabry–Perot cavity lasers, starting with the well known Tang–Statz–de Mars model [25]. We refer the interested reader to [12, 26, 27, 28] and references therein. That subject, while very interesting in itself, is beyond the scope of the present discussion.

²Interestingly, in 1976 Graham [33] showed that the multimode laser model, the RNGH model, is isomorphous to the Lorenz model [16], thus extending the analogy discovered by Haken the previous year [15]. The difference between the singlemode and the multimode case is that in the latter the parameter σ is not fixed as it depends on the velocity of the travelling-wave solution. This would be extended further to cover detuning in 1990 when Ning and Haken [34] showed that the detuned multimode laser equations are isomorphic to the complex Lorenz model for the baroclinic instability [35]. This isomorphism is a powerful tool that has not been investigated enough, specially for what concerns the multimode instability.

at least nine times the lasing threshold (the same “factor-of-nine” as in single-mode instabilities in the Lorenz–Haken model). Another condition was that the laser cavity length must exceed a certain minimum. Indeed, it has to be unrealistically long for conventional bulk lasers [2, 9].

Due to these predictions and without experimental demonstration of the opposite, interest in RNGHI abated over time: While during the Seventies and Eighties much theoretical effort was devoted to the understanding of the RNGHI as well as to the dynamics of the laser above the second threshold [36, 37, 38, 39, 40, 41, 42, 43], eventually RNGHI was more or less dismissed as a merely academical prediction rather than an actual mechanism for multimode emission.

In 1984 researchers announced that they had observed what could be interpreted as RNGHI in a dye laser [44, 45]. The dye laser seemed to be a good candidate for the observation of the RNGHI as (i) it is a homogeneously broadened laser, and (ii) the “critical” cavity length (see later for a precise definition of this term) is smaller than typical resonator lengths [2]. However, it was peculiar that in the spectrum there were only two peaks instead of three. Finally, after some debate [46], Fu and Haken showed that a suitable model for the dye (consisting of bands rather than levels) could explain the observations without invoking the RNGHI [47, 48, 49]. From then on the observation in [44, 45] was no longer considered as a manifestation of the RNGHI.

A few years later, a phenomenon very similar to RNGHI was discussed in the context of optical bistability performed in the microwave regime [50, 51]. The experimental system consisted of a waveguide Fabry–Perot cavity with a length of 182 m filled with hydrocyanic acid vapor at low (≈ 1 mTorr) pressure. Driven at a frequency of 86 GHz near a HC^{15}N transition, this system displayed bistability and, on the upper branch of the bistable loop, self-oscillation at a frequency of the order of the cavity free spectral range and of the Rabi frequency, but could deviate by 50% or so. Nevertheless it is to be emphasized that this fairly unique experiment actually displayed not the RNGHI, but the multimode instability of optical bistability predicted in 1978 by Bonifacio and Lugiato [52]. Thus, for many years and after a false start, the closest thing to the RNGHI laser instability that was actually observed was Rabi splitting in microwave optical bistability – not very close, certainly.

The discussion on the RNGHI during the late Eighties and the Nineties faded, although theoretical studies continued [32, 53, 54, 55, 56, 57, 58, 59, 60, 61, 62, 63, 64, 65, 66, 67, 68], and signatures of the RNGHI were predicted also for laser related systems such as a laser with an intracavity parametric amplifier [69], and a laser with injected signal [70]. Nonetheless, in this period it seemed like the matter of longitudinal mode instabilities in lasers, and the RNGHI in particular, would soon be more or less forgotten.

The situation changed with a suggestion by Lugiato and coworkers [71, 72]. They observed that a ring-cavity erbium-doped fibre laser (EDFL) spontaneously mode-locked and emitted a train of pulses with a repetition time equal to the cavity roundtrip time. This is one signature of the RNGHI, but certainly not in itself a sufficient criterion. However, the unusually long cavity length of fibre lasers automatically fulfils the most difficult prerequisite for RNGHI of

sufficient resonator length. On this basis they put forward the hypothesis that self-pulsing in these lasers could be a manifestation of the RNGHI (see also [73] for compatible experimental results).

Unfortunately they could not confirm the existence of a second laser threshold, *i.e.* a threshold-like onset of the instability. Moreover, there was a grave quantitative difficulty: Instabilities were observed at pump powers immediately above the lasing threshold [72], in stark contrast to the prediction that the second threshold be at least nine times higher than the first.

It was subsequently shown that this requirement is not necessarily applicable to real-world lasers. In [74] the usual two-level atom model for Lorenz-type instability was extended to incorporate a third level as a necessity for applying a pump source. It turned out that the instability threshold was lowered such as to come close to the lasing threshold. This finding was then applied to EDFLs [75]. Erbium ions, too, behave more like three-level systems [76], rather than two-level systems as the original theory assumed. Now the ratio of the instability to the laser threshold was predicted to be close to unity. This was subsequently corroborated (and expanded to include four-level cases) in [77].

Put simply, for EDFLs the expected “factor-of-nine”, became a “factor-of- $(1 + \epsilon)$ ”. Thereby, the apparent contradiction with the hypothesis in [72] is gone. This insight bestowed fresh vigor on the debate on RNGHI and led to dedicated experimental investigation as will be described below.

In this paper we shall review the fundamentals of the RNGH theory as well as the research we have carried out along the recent years (including some inedit results), *i.e.*, we shall not review in detail the available literature. After this historical introduction, the paper follows with three more sections. Sect. 2 is devoted to the RNGHI in homogeneously broadened media. In this section we first explain in detail modelling issues, Sect. 2.1, and then we treat the RNGHI, first in the uniform field limit (Sect. 2.2) and then outside the limit of validity of this standard approximation (Sect. 2.3). In Sect. 3 we consider multilongitudinal mode emission in inhomogeneously broadened media, again within (Sect. 3.2) and outside (Sect. 3.3) the uniform field limit. Then in Sect. 4 we discuss the experimental aspects of the RNGHI concentrating our discussion on erbium-doped fibre lasers. Finally, in Sect. 5 we provide a general discussion of the issue.

2 MULTILONGITUDINAL MODE EMISSION IN HOMOGENEOUSLY BROADENED RING LASERS: THE RNGH INSTABILITY

2.1 Modelling

In this section we introduce the standard two-level laser theory (Sect. 2.1.1). We then discuss how the model can be applied to three- and four-level lasers (Sect. 2.1.2), and how it can be generalized to treat the dependence of the

laser field and of the pump field on the radial coordinate (Sect. 2.1.3). Finally, we determine the stationary singlemode solutions of the laser equations (Sect. 2.1.4, and we rigorously derive the laser equations in the uniform field limit (Sect. 2.1.5).

2.1.1 Two-level atoms

We consider a collection of \mathcal{N} two-level homogeneously broadened atoms per unit volume, with transition frequency ω_a interacting with a linearly polarized, plane wave, unidirectional electric field of carrier frequency ω_c , chosen as the longitudinal mode frequency closest to ω_a . The Maxwell-Bloch equations describing the system are [9, 11, 12, 46, 78]

$$\partial_z F + v_m^{-1} \partial_t F = \frac{a}{2} P - \frac{\alpha_m}{2} F, \quad (1)$$

$$\partial_t P = \gamma_\perp [FD - (1 + i\delta)P], \quad (2)$$

$$\partial_t D = \gamma_\parallel [1 - D - \text{Re}(F^*P)]. \quad (3)$$

Here F , P and D are properly scaled variables representing the electric field, medium polarization, and population difference

$$F = \frac{2E}{\sqrt{\gamma_\perp \gamma_\parallel}}, \quad P = -2i \frac{\rho_{12}}{d_0} \sqrt{\frac{\gamma_\perp}{\gamma_\parallel}}, \quad D = \frac{d}{d_0}. \quad (4)$$

In these expressions E is the Rabi frequency associated with the laser field, ρ_{12} is the slowly varying envelope of the coherence between the lasing levels, and d is the population difference per atom between the upper (2) and lower (1) lasing levels; γ_\perp and γ_\parallel are the decay rates of the medium polarization and population difference, respectively, $\delta = (\omega_a - \omega_c)/\gamma_\perp$ is the detuning between the atoms and the cavity, $v_m = c/n_m$ is the light velocity in the host medium with refractive index n_m , α_m is an intensity loss coefficient per unit length, which describes (non resonant) distributed losses inside the active medium [78], and d_0 is the equilibrium value towards which d relaxes in the absence of an electric field. d_0 is positive because the medium is amplifying. The unsaturated intensity gain coefficient per unit length a is proportional to the total population difference $\mathcal{N}d_0$, and we can write it as

$$a = \frac{4\pi\mu^2\omega_c}{ch\gamma_\perp} \mathcal{N}d_0, \quad (5)$$

where μ is the dipole moment between the two levels of the laser transition.

Equations (1)–(3) must be supplied with the appropriate boundary condition for the electric field. We assume that the active medium fills a region of length L_m inside a ring cavity of length L_c . Denoting by $z = 0$ and $z = L_m$ the entrance and exit planes of the amplifying medium, the electric field obeys the boundary condition

$$F(0, t) = \mathcal{R}F(L_m, t - \Delta t), \quad (6)$$

where \mathcal{R} is the effective cavity reflectivity³, $\Delta t = (L_c - L_m)/v_c$, and $v_c = c/n_c$ is the speed of light within the unloaded part of the cavity, whose refractive index is n_c .

A standard procedure to make the boundary condition isochronous consists in defining the new spatial and temporal variables [46]

$$Z = \frac{z}{L_m}, \quad T = t + \frac{z}{L_m} \Delta t. \quad (7)$$

This transformation amounts to ideally bend the active medium so that its entrance and exit coincide, and the delay Δt accumulated in the trivial propagation outside the amplifying medium is removed. The boundary conditions now read

$$F(0, T) = \mathcal{R}F(1, T), \quad (8)$$

and the Maxwell–Bloch equations become

$$\left(\partial_T + \frac{\alpha_{\text{FSR}}}{2\pi} \partial_Z \right) F = \kappa (AP - \chi F), \quad (9)$$

$$\partial_T P = \gamma_{\perp} [FD - (1 + i\delta)P], \quad (10)$$

$$\partial_T D = \gamma_{\parallel} [1 - D - \text{Re}(F^*P)], \quad (11)$$

where $\alpha_{\text{FSR}} = 2\pi c/\mathcal{L}_c$ is the cavity free spectral range,

$$\kappa = \frac{c}{2\mathcal{L}_c} (|\ln \mathcal{R}^2| + \alpha_m L_m), \quad (12)$$

is the cavity linewidth, $\mathcal{L}_c = n_m L_m + n_c(L_c - L_m)$ is the optical length of the cavity, and

$$A = \frac{aL_m}{|\ln \mathcal{R}^2| + \alpha_m L_m} \quad (13)$$

is the adimensional pump parameter, while

$$\chi = \frac{\alpha_m L_m}{|\ln \mathcal{R}^2| + \alpha_m L_m}, \quad (14)$$

$0 \leq \chi \leq 1$, is an adimensional loss parameter due to distributed losses inside the amplifying medium. In the absence of distributed loss ($\alpha_m = 0$), $\chi = 0$, and the pump parameter becomes $A = aL_m/|\ln \mathcal{R}^2|$, which is its usual definition.

In the RNGHI for class B lasers it is known that instability occurs when the cavity free spectral range is a quantity of order $\sqrt{\gamma_{\parallel}\gamma_{\perp}}$ [31] (see below). In view of this, it is convenient to introduce the new temporal and spatial variables

$$\tau = \sqrt{\gamma_{\parallel}\gamma_{\perp}} T, \quad \zeta = \frac{2\pi}{\tilde{\alpha}} Z, \quad (15)$$

³ \mathcal{R} accounts for all localized intracavity losses occurring outside the active medium (at splices, filters, output couplers, or other components). Namely, $\mathcal{R}^2 = \mathcal{R}_1^2 \cdot \mathcal{R}_2^2 \dots \mathcal{R}_n^2$, where \mathcal{R}_i^2 is the fraction of power after the i -th lossy element. Distributed losses outside the amplifying medium which damp the intensity of the electric field at a rate α_{out} can also be included in the effective reflectivity \mathcal{R} by multiplying it with $\exp[-\alpha_{\text{out}}(L_c - L_m)/2]$.

where

$$\tilde{\alpha} = \frac{\alpha_{\text{FSR}}}{\sqrt{\gamma_{\parallel}\gamma_{\perp}}} = \frac{2\pi c}{\mathcal{L}_c \sqrt{\gamma_{\parallel}\gamma_{\perp}}}, \quad (16)$$

is the scaled free spectral range. If we define also the adimensional decay rates

$$\sigma = \frac{\kappa}{\sqrt{\gamma_{\parallel}\gamma_{\perp}}}, \quad \gamma = \sqrt{\frac{\gamma_{\parallel}}{\gamma_{\perp}}}, \quad (17)$$

the Maxwell–Bloch equations read

$$(\partial_{\tau} + \partial_{\zeta})F = \sigma(AP - \chi F), \quad (18)$$

$$\partial_{\tau}P = \gamma^{-1}[FD - (1 + i\delta)P], \quad (19)$$

$$\partial_{\tau}D = \gamma[1 - D - \text{Re}(F^*P)], \quad (20)$$

with the boundary condition

$$F(0, \tau) = \mathcal{R}F(\zeta_m, \tau), \quad (21)$$

where

$$\zeta_m = \frac{2\pi}{\tilde{\alpha}} \quad (22)$$

is the position of the exit plane of the amplifying medium in the space variable ζ . Note the following useful relation

$$2\sigma\zeta_m(1 - \chi) = |\ln \mathcal{R}^2|. \quad (23)$$

2.1.2 Three- and four-level atoms

Real lasers are not two-level lasers, even those in which the lasing transition can be well described as a two-level system. This is so because pump and relaxation processes connect, incoherently, the two lasing levels to some other levels. Although under usual conditions (essentially when the relaxation rates of the pumped transition are very large as compared with the rest of relaxation rates) this incoherent coupling does not have any influence on the coherent dynamics of the system, it turns out to be essential for understanding the meaning of the laser parameters, particularly that of the pump parameter A . The connection between the two-level theory and the description of three- and four-level lasers (which are the usual schemes for describing real lasers) was first treated, to the best of our knowledge, by Khanin in his book [11], but he did not analyze the consequences of the parameter transformations he derived. Later on, and independently of Khanin, these transformations were derived again in [77]⁴, and their influence on the understanding of laser dynamics was clarified. The relation between two-level and three- and four-level lasers is important in our context because we will apply our analysis especially to rare-earth doped fibre

⁴In [77] equal relaxation rates for the two lasing levels in four-level lasers were assumed. This is not a realistic approximation for Nd:YAG lasers. In [79], following [11], it was shown that the same model can be derived even removing that assumption

lasers, where the active medium should be properly modelled as a collection of three- or four-level atoms if the dopants are, respectively, Erbium or Neodymium atoms [76].

Eqs. (18–20), describing two-level lasers, are valid also for three- and four-level atoms provided a dependence on the rate of incoherent optical pumping W_{opt} is included in the parameters γ_{\parallel} and d_0 [77, 79]. Precisely, we define the adimensional pumping rate

$$W = \frac{W_{\text{opt}}}{\gamma_2}, \quad (24)$$

where γ_2 is the total spontaneous decay rate from the upper level of the lasing transition. Then, the parameter transformation necessary for applying Eqs. (18–20) to three- and four-level lasers are

$$\gamma_{\parallel} = \gamma_2(1 + W), \quad (25)$$

and

$$d_0 = \frac{W - \delta_{N,3}}{W + 1}, \quad (26)$$

where $\delta_{N,3}$ is the Kroenecker δ and N is the number of atomic levels. Thus, $\delta_{N,3} = 1$ for three-level atoms, and $\delta_{N,3} = 0$ for four-level atoms.

In fibre lasers the gain parameter a is usually defined in a way different from Eq. (5). If σ_e and σ_a are, respectively, the stimulated emission and absorption cross sections, one has [76]

$$a = \frac{\mathcal{N}}{2} [\sigma_e - \sigma_a + (\sigma_e + \sigma_a)d_0]. \quad (27)$$

Assuming $\sigma_e = \sigma_a$, the gain coefficient turns out to be proportional to the equilibrium total population difference per unit volume $\mathcal{N}d_0$, as in Eq. (5)

$$a = \sigma_e \mathcal{N} d_0. \quad (28)$$

Under this approximation, taking into account the definition of the pump parameter A , Eq. (13), and Eq. (26), the dependence of the pump parameter on the pumping rate W can be expressed in the following way

$$A = G \frac{W - \delta_{N,3}}{W + 1}, \quad (29)$$

with

$$G = \frac{G_0}{|\ln \mathcal{R}^2| + \alpha_m L_m}, \quad G_0 = \mathcal{N} \sigma_e L_m. \quad (30)$$

Notice that γ_{\parallel} enters in the normalizations used for writing Eqs. (18–20), and as this parameter is pump dependent in the case of three- and four-level lasers, Eq. (25), this must be taken into account when interpreting the results derived from Eqs. (18–20). The recipe is very simple: (i) replace A by using Eq. (29), and (ii) replace the spatial frequency α by $\alpha\sqrt{1+W}$ in the final expressions

(see following sections). This last replacement is due to the normalization of the axial coordinate and, consequently, of the spatial frequency, see Eq. (16).

The most relevant feature of Eq. (29) is that the effective two-level pump parameter A depends on the actual pump strength W in a non-linear fashion for both three- and four-level lasers. Although the instability threshold will be discussed below, let us comment that for three-level lasers the relationship between A and W and the fact that usually $G \gg 1$ imply that the “factor-of-nine” (the ratio of A at the RNGHI instability threshold and at the laser threshold) (see Sect. 2.2.2 below) becomes a “factor of $(1 + \epsilon)$ ” for W , which is the actual pump parameter that can be measured in an experiment [77]. This is very easy to see: From Eq. (29)

$$W = \frac{G + A}{G - A}, \quad (31)$$

and then, the instability to lasing threshold

$$\left(\frac{W_{\text{ins}}}{W_0} \right)_{3\text{L}} = \frac{G + 9}{G - 9} / \frac{G + 1}{G - 1} \rightarrow 1 + \frac{16}{G}, \quad (32)$$

where the limit holds for large G . Contrarily, the case of four-level lasers is very similar to that of two-level lasers as in this case

$$\left(\frac{W_{\text{ins}}}{W_0} \right)_{4\text{L}} = \frac{9}{G - 9} / \frac{1}{G - 1} \rightarrow 9 + \frac{72}{G},$$

where the limit corresponds to large G again. We see that the instability threshold for four-level lasers is larger than that of two-level lasers, tending to it for very large gain.

2.1.3 Transverse effects

So far we have limited our analysis to the plane wave approximation. However, transverse effects may play an important role in real experimental situations. In fibre lasers, for instance, both the laser and pump field have a transverse spatial structure and the doped region has a finite extension [76].

To include these elements in the laser equations we first notice that the definitions of the dynamical variables F , P and D , Eq. (4), are no longer appropriate, because such definitions contain the parameters γ_{\parallel} and d_0 which depend on the pump W . If W is allowed to vary spatially, this introduces an undesired spatial dependence in the dynamical variables. The problem can be removed by introducing a new definition of F , P and D

$$F = \frac{2E}{\sqrt{\gamma_{\perp}\gamma_2}}, \quad P = -2i\rho_{12}\sqrt{\frac{\gamma_{\perp}}{\gamma_2}}, \quad D = d. \quad (33)$$

The dynamical variables do not depend on W any longer, and they obey the

dynamical equations

$$(\partial_\tau + \partial_\zeta) F = \sigma (GP - \chi F) , \quad (34)$$

$$\partial_\tau P = \gamma^{-1} [FD - (1 + i\delta)P] , \quad (35)$$

$$\partial_\tau D = \gamma [W(1 - D) - \delta_{N,3} - D - \text{Re}(F^*P)] , \quad (36)$$

where in σ and γ , as well as in the free spectral range $\tilde{\alpha}$, the decay rate γ_{\parallel} is replaced by γ_2 .

Now we must include in these equations the dependence of the electric field F on the transverse coordinate. We assume that the laser field is a Gaussian beam with $1/e$ radius equal to w_0 , which is a fairly good approximation [76]. This implies that in the Maxwell–Bloch equations all the dynamical variables depend also on the radial coordinate r through the scaled coordinate $\rho = r/w_0$, and in the equation for the electric field a term describing diffraction must be included

$$-\frac{i}{4\zeta_0} \nabla^2 F + (\partial_\tau + \partial_\zeta) F = \sigma (GP - \chi F) . \quad (37)$$

Here $\nabla^2 = \partial^2/\partial\rho^2 + (1/\rho)(\partial/\partial\rho)$ is the transverse part of the Laplacian and ζ_0 is the scaled Rayleigh length of the beam *i.e.* the distance in the propagation direction over which the size of the beam varies appreciably. A Gaussian beam is described by the function [23, 24]

$$\psi(\rho, \zeta) = \frac{1}{w(\zeta)} \exp \left[-\frac{\rho^2}{w^2(\zeta)} + i \frac{\rho^2}{w^2(\zeta)} \frac{\zeta}{\zeta_0} - i \arctan \left(\frac{\zeta}{\zeta_0} \right) \right] , \quad (38)$$

with $w^2(\eta) = 1 + (\zeta/\zeta_0)^2$, which is a solution of the empty cavity equation

$$\frac{i}{4\zeta_0} \nabla^2 \psi = \partial_\zeta \psi . \quad (39)$$

We can write the electric field as $F(\rho, \zeta, \tau) = \psi(\rho, \zeta)f(\zeta, \tau)$ and, taking into account the normalization property of ψ

$$\int_0^\infty d\rho \rho |\psi(\zeta, \rho)|^2 = \frac{1}{4} , \quad (40)$$

valid for any ζ , we can project the equation for the total field F on the mode amplitude f by multiplying each term by ψ^* and integrating over ρ from 0 to ∞

$$(\partial_\tau + \partial_\zeta) f = \sigma \left(4G \int_0^\infty d\rho \rho e^{-\rho^2} P - \chi f \right) . \quad (41)$$

Here we have also assumed $\zeta \ll \zeta_0$, so that the dependence on ζ of ψ can be neglected, and $\psi(\rho) = \exp(-\rho^2)$. We make the same assumption for the pump field, and we denote its maximum amplitude by $\beta^{1/2}$ and its $1/e$ radius by w_p . Introducing the parameter $\eta = (w_0/w_p)^2$, the pump term, which is proportional to the intensity of the pump field, can be written as $W(\rho) = \beta \exp(-2\eta\rho^2)$. Finally, we replace f again with F and introduce the new radial coordinate

$u = 2\rho^2$. The Maxwell–Bloch equations suitable to describe transverse effects read

$$(\partial_\tau + \partial_\zeta) F = \sigma \left(G \int_0^{u_m} du e^{-u/2} P - \chi F \right), \quad (42)$$

$$\partial_\tau P = \gamma^{-1} \left[e^{-u/2} F D - (1 + i\delta) P \right], \quad (43)$$

$$\partial_\tau D = \gamma \left[\beta e^{-\eta u} (1 - D) - \delta_{N,3} - D - e^{-u/2} \text{Re}(F^* P) \right], \quad (44)$$

with the boundary condition

$$F(0, u, \tau) = \mathcal{R}F(\zeta_m, u, \tau), \quad \zeta_m = 2\pi/\tilde{\alpha}. \quad (45)$$

We have fixed the upper limit in the integral over the radial coordinate equal to $u_m = 2(r_m/w_0)^2$, where r_m is the radius of the amplifying medium. In the case of a fibre r_m coincides with the radius of the doped region.

2.1.4 Stationary singlemode solutions

We now return to the Maxwell–Bloch equations (18)–(20) in the plane wave approximation and look for their single frequency (singlemode) solutions, which can be found by setting

$$F(\zeta, \tau) = F_s(\zeta) e^{-i\omega\tau}, \quad P(\zeta, \tau) = P_s(\zeta) e^{-i\omega\tau}, \quad D(\zeta, \tau) = D_s(\zeta).$$

The stationary atomic variables are

$$P_s = \frac{1 - i\Delta}{1 + \Delta^2 + |F_s|^2} F_s, \quad (46)$$

$$D_s = \frac{1 + \Delta^2}{1 + \Delta^2 + |F_s|^2}, \quad (47)$$

where $\Delta \equiv \delta - \gamma\omega$ and F_s verifies the differential equation

$$\frac{dF_s}{d\zeta} = \sigma (AP_s - \chi F_s) + i\omega F_s.$$

Using the polar decomposition $F_s = I_s^{1/2} e^{i\phi_s}$ and splitting the above equation into its real and imaginary parts, one obtains

$$\frac{dI_s}{d\zeta} = 2\sigma \left(\frac{A}{1 + \Delta^2 + I_s} - \chi \right) I_s, \quad (48)$$

$$\frac{d\phi_s}{d\zeta} = \omega - \frac{\sigma\Delta A}{1 + \Delta^2 + I_s}, \quad (49)$$

with the boundary conditions

$$I_s(0) = \mathcal{R}^2 I_s(\zeta_m), \quad (50)$$

$$\phi_s(\zeta_m) - \phi_s(0) = 2\pi n, \quad n \text{ integer}. \quad (51)$$

Integration of Eq. (48) yields

$$(1 + \Delta^2) \ln \frac{I_s(\zeta)}{I_s(0)} - \frac{A}{\chi} \ln \frac{A - \chi [1 + \Delta^2 + I_s(\zeta)]}{A - \chi [1 + \Delta^2 + I_s(0)]} = [A - \chi (1 + \Delta^2)] 2\sigma\zeta. \quad (52)$$

Particularizing this equation to $\zeta = \zeta_m$ and taking into account Eqs. (23) and (50), we find that the stationary intensity at the exit of the active medium is

$$I_s(\zeta_m) = \left(\frac{A}{\chi} - 1 - \Delta^2 \right) \frac{1 - \exp \left[- |\ln \mathcal{R}^2| \frac{\chi}{1-\chi} \frac{A-1-\Delta^2}{A} \right]}{1 - \mathcal{R}^2 \exp \left[- |\ln \mathcal{R}^2| \frac{\chi}{1-\chi} \frac{A-1-\Delta^2}{A} \right]}. \quad (53)$$

It can be easily seen that the lasing threshold, *i.e.* the value of A for which $I_s(\zeta_m) = 0$, is $1 + \Delta^2$. In the limit of no distributed losses ($\chi \rightarrow 0$) Eq. (53) reduces to

$$I_s(\zeta_m) = \frac{|\ln \mathcal{R}^2|}{1 - \mathcal{R}^2} [A - (1 + \Delta^2)], \quad (\chi = 0). \quad (54)$$

The frequency ω of the lasing solution has still to be fixed. To do that we must determine how the stationary phase ϕ_s varies along ζ . If we insert Eq. (48) into Eq. (49), the latter can be written as

$$\frac{d\phi_s}{d\zeta} = \omega - \sigma\Delta\chi - \frac{\Delta}{2I_s} \frac{dI_s}{d\zeta}. \quad (55)$$

from which it follows that ϕ_s depends on ζ in a nonlinear way as

$$\phi_s(\zeta) - \phi_s(0) = (\omega - \sigma\Delta\chi)\zeta - \frac{\Delta}{2} \ln \frac{I_s(\zeta)}{I_s(0)}. \quad (56)$$

The total phase shift experienced by the field in a roundtrip from 0 to ζ_m is then

$$\phi_s(\zeta_m) - \phi_s(0) = (\omega - \sigma\Delta)\zeta_m = (\omega - \sigma\delta + \sigma\gamma\omega) \frac{2\pi}{\tilde{\alpha}}, \quad (57)$$

where we have used Eqs. (23) and (22) and the fact that $\Delta = \delta - \gamma\omega$. Imposing the boundary condition (51), we obtain for the n -th longitudinal mode

$$\omega_n = \frac{n\tilde{\alpha} + \sigma\delta}{1 + \gamma\sigma}, \quad \Delta_n = \frac{\delta - \gamma n\tilde{\alpha}}{1 + \gamma\sigma}. \quad (58)$$

The singlemode solution associated with the n -th mode has threshold $1 + \Delta_n^2$. Recalling that $\delta = (\omega_a - \omega_c)/\gamma_\perp$, and that $|\omega_a - \omega_c| \leq \alpha_{\text{FSR}}/2$ by definition (α_{FSR} is the cavity free spectral range), we have $|\delta| \leq \frac{1}{2}\gamma\tilde{\alpha}$. Hence, the mode with the lowest threshold is the one with $n = 0$, according to our initial choice of the reference frequency. For this mode

$$\omega_0 = \frac{\sigma\delta}{1 + \gamma\sigma} = \frac{\kappa\omega_a + \gamma_\perp\omega_c}{\kappa + \gamma_\perp}, \quad \Delta_0 = \frac{\delta}{1 + \gamma\sigma} = \frac{\omega_a - \omega_c}{\kappa + \gamma_\perp}. \quad (59)$$

The expression for ω_0 corresponds to the well-known mode pulling formula. From now on $\Delta = \Delta_0$ will be our laser-atoms detuning parameter, and the condition of perfectly resonant laser will be equivalent to $\Delta = 0$.

2.1.5 The uniform field limit

A widely adopted approximation in the study of laser dynamics is the so-called Uniform Field Limit (UFL), which is based on the assumption that the steady state of the electric field is nearly constant along the propagation direction inside the amplifying medium. In other words, in the uniform field limit the electric field obeys a periodic boundary condition, as if the cavity mirrors were perfectly reflecting. From the analytic point of view this represents a great simplification of the problem, because it allows for an expansion of the electric field in terms of the Fourier modes $\exp(i\alpha_n\zeta)$ of the empty cavity, where $\alpha_n = n\tilde{\alpha}$ is the frequency of the n -th mode and the singlemode stationary solution associated with mode $n = 0$ is spatially homogeneous. From the numerical point of view, the benefits of the UFL are even more relevant, because the expansion of electric field in Fourier modes allows to transform the original set of Maxwell-Bloch equations from partial differential equations to ordinary differential equations, which can be numerically integrated much easier and faster. Although our work on the RNGHI shows that the above mentioned features of the UFL persist even outside that limit for class B lasers (see Sect. 2.3), in the most complex situations – for instance when transverse effects or inhomogeneous broadening are included in the model – we still limit our analysis to the UFL for the sake of algebraic simplicity.

In [80] we introduced a new technique for dealing with the UFL. In comparison to the standard technique [56], the new technique is advantageous because it allows to clearly demonstrate that the only requirement for applying the UFL is that the resonator reflectivity must be close enough to unity (the single-pass gain does not have to verify any constraint). In [80] the simplest case of exact resonance and absence of distributed loss was considered. In this section we show, following [80], how the Maxwell-Bloch equations in the UFL can be derived for homogeneously broadened lasers in the plane wave approximation in the presence of both detuning and distributed loss. The generalization to other situations (including, e.g., transverse effects or inhomogeneous broadening) is straightforward.

To derive the dynamical equations in the UFL we first observe that in the limit $\mathcal{R}^2 \rightarrow 1$ the solution of Eq. (52) for the n -th mode varies slowly along ζ according to the equation

$$I_s(\zeta) = [A - (1 + \Delta_n^2)] \left[1 + \mathcal{T} \left(\frac{\zeta}{\zeta_m} - \frac{1}{2} \right) \right] + \mathcal{O}(\mathcal{T}^2), \quad (60)$$

where $\mathcal{T} \equiv 1 - \mathcal{R}^2$ is a small parameter. We thus see that, independently of the value of all other laser parameters, the laser intensity is almost uniform along the active medium in the limit $\mathcal{R}^2 \rightarrow 1$, hence the name UFL. If we insert the above expression for $I_s(\zeta)$ in Eq. (56), and take into account Eqs. (23) and (58), we find that the stationary phase also varies linearly along ζ according to the simple expression

$$\phi_s(\zeta) - \phi_s(0) = n\tilde{\alpha}\zeta + \mathcal{O}(\mathcal{T}^2), \quad (61)$$

which shows that the space frequency associated with the n -th solution is $n\tilde{\alpha}$. We focus on the $n = 0$ solution for which the stationary phase is constant along ζ . Thus, in the UFL, this stationary solution can be written as

$$\begin{aligned} I_s^{\text{UFL}} &= A - 1 - \Delta^2, & F_s^{\text{UFL}} &= \sqrt{I_s^{\text{UFL}}} e^{i\phi}, \\ P_s^{\text{UFL}} &= \frac{1-i\Delta}{A} F_s^{\text{UFL}}, & D_s^{\text{UFL}} &= \frac{1+\Delta^2}{A}. \end{aligned} \quad (62)$$

Now we introduce new dynamical variables obtained from the old ones dividing them by the stationary solution $n = 0$ outside the UFL and multiplying by the same solution in the UFL

$$F'(\zeta, \tau) = \frac{F(\zeta, \tau)}{F_s(\zeta)e^{-i\omega\tau}} F_s^{\text{UFL}}, \quad (63)$$

$$P'(\zeta, \tau) = \frac{P(\zeta, \tau)}{P_s(\zeta)e^{-i\omega\tau}} P_s^{\text{UFL}} = \frac{F_s^{\text{UFL}}}{\eta(\zeta)} \frac{P(\zeta, \tau)}{F_s(\zeta)e^{-i\omega\tau}}, \quad (64)$$

$$D'(\zeta, \tau) = \frac{D(\zeta, \tau)}{D_s(\zeta)} D_s^{\text{UFL}} = \frac{D(\zeta, \tau)}{\eta(\zeta)}, \quad (65)$$

with

$$\eta(\zeta) = \frac{1 + \Delta^2 + I_s^{\text{UFL}}}{1 + \Delta^2 + I_s(\zeta)} = \frac{A}{1 + \Delta^2 + I_s(\zeta)}. \quad (66)$$

Since $F_s(0) = \mathcal{R}F_s(\zeta_m)$, the new electric field $F'(\zeta, \tau)$ obeys a *periodic* boundary condition

$$F'(0, \tau) = F'(\zeta_m, \tau). \quad (67)$$

The Maxwell-Bloch equations (18–20) for the primed variables take the form

$$(\partial_\tau + \partial_\zeta)F' = \sigma\eta(\zeta)[AP' - (1 - i\Delta)F'], \quad (68)$$

$$\partial_\tau P' = \gamma^{-1}[F'D' - (1 + i\Delta)P'], \quad (69)$$

$$\partial_\tau D' = \gamma \left[\frac{1}{\eta(\zeta)} - D' - \frac{I_s(\zeta)}{I_s^{\text{UFL}}} \text{Re}(F'^* P') \right]. \quad (70)$$

Because of the periodicity condition (67) these equations are particularly suitable for numerical integration, as we shall discuss in Sect. 2.3.5.

Obviously, Eqs. (68–70) admit as a stationary solution the UFL stationary solution (62). Yet, they are still equivalent to the original Maxwell–Bloch equations, and this fact is reflected in the dependence on ζ of η and I_s . But from Eqs. (60), (62), and (66) we see that in the UFL

$$\frac{I_s(\zeta)}{I_s^{\text{UFL}}} = 1 + \mathcal{T} \left(\frac{\zeta}{\zeta_m} - \frac{1}{2} \right) + \mathcal{O}(\mathcal{T}^2). \quad (71)$$

$$\eta(\zeta) = 1 + \frac{A - 1 - \Delta^2}{A} \mathcal{T} \left(\frac{\zeta}{\zeta_m} - \frac{1}{2} \right) + \mathcal{O}(\mathcal{T}^2), \quad (72)$$

Thus, in the very limit we can set both terms equal to unity, and, dropping the primes, the laser equations in the UFL take the well-known form

$$(\partial_\tau + \partial_\zeta)F = \sigma[AP - (1 - i\Delta)F], \quad (73)$$

$$\partial_\tau P = \gamma^{-1}[FD - (1 + i\Delta)P], \quad (74)$$

$$\partial_\tau D = \gamma[1 - D - \text{Re}(F^* P)], \quad (75)$$

with the boundary condition

$$F(0, \tau) = F(\zeta_m, \tau), \quad \zeta_m = 2\pi/\tilde{\alpha}. \quad (76)$$

These equations differ from the general ones (Eqs. (18)–(21)) only in one respect: The (localized) cavity losses, represented by the mirror reflectivity \mathcal{R} , have disappeared from the boundary condition (which now is periodic) and have appeared in the dynamical equation for the electric field through the term $-\sigma F$, which contains *both localized and distributed losses*. The appearance of a detuning in the equation for F as well as the replacement of δ with Δ in the equation for P are only apparent changes, due to the fact that in Eqs. (73–75) the reference frequency is the lasing frequency ω_0 , while in Eqs. (18)–(20) the reference frequency is the empty cavity frequency ω_c .

Let us stress that to derive the Maxwell–Bloch equations in the UFL we had *only* to assume that $\mathcal{R}^2 \rightarrow 1$. Eqs. (71–72) show that this assumption suffices to approximate $I_s(\zeta)/I_s^{\text{UFL}}$ and $\eta(\zeta)$ with unity, for *any* value of the pump parameter A greater than one, no matter how large it is. Therefore, the condition of small single pass gain $aL_m \rightarrow 0$, which invariably accompanies the condition $\mathcal{R}^2 \rightarrow 1$ in the literature about the UFL, is actually completely superfluous. Notice also that the amount of distributed loss does not influence the validity of the UFL.

2.2 The RNGH instability in the uniform field limit

The uniform field limit (UFL), rigorously introduced in Sect. 2.1.5, is the case in which the RNGHI can be analyzed in the simplest way, as well as the limit where the effects of additional features not considered in the original analyzes by Risken and Nummedal [29] and by Graham and Haken [30] can be studied most easily. Still another reason for the interest in the UFL is that it still captures the very basic signatures of the multimode instability of ring lasers found in more complex models.

In this section, we shall first derive again the classical results of RNGH (Sect. 2.2.1). Then we shall consider the relevant case when the population inversion is an extremely slow variable (class B laser). This applies, in particular, to fiber lasers (Secs. 2.2.2 and 2.2.3). Next we will show that detuning plays no role in class B lasers (Sect. 2.2.4). Finally, we shall analyze the spatial (transverse) effects due to the modal structure of fiber lasers (Sect. 2.2.5).

2.2.1 The RNGH instability

The original studies by RNGH [29, 30] considered a perfectly resonant two–level ring laser in the UFL. The Maxwell–Bloch equations that describe such laser are given by Eqs. (73)–(75) introduced in Sect. 2.1.5 with $\Delta = 0$

$$(\partial_\tau + \partial_\zeta)F = \sigma(AP - F), \quad (77)$$

$$\partial_\tau P = \gamma^{-1}(FD - P), \quad (78)$$

$$\partial_\tau D = \gamma[1 - D - \text{Re}(F^*P)], \quad (79)$$

supplemented by the *periodic* boundary condition

$$F(0, \tau) = F(\zeta_m, \tau), \quad \zeta_m = 2\pi/\tilde{\alpha}. \quad (80)$$

The steady, *spatially uniform*, lasing solution is given by Eq. (62) with $\Delta = 0$

$$F_s = \sqrt{A-1} e^{i\phi}, \quad P_s = \frac{F_s}{A}, \quad D_s = \frac{1}{A}, \quad (81)$$

where ϕ is an arbitrary phase, and it exists for $A > 1$ ($A = 1$ corresponds to the first laser threshold). This solution is the basic, singlemode lasing solution. Other singlemode solutions exist (in fact an infinite countable set) that can be obtained from Eqs. (77)–(80) by setting $F(\zeta, \tau) = F_{s,n} \exp[i(n\tilde{\alpha}\zeta - \omega_n\tau)]$, $P(\zeta, \tau) = P_{s,n} \exp[i(n\tilde{\alpha}\zeta - \omega_n\tau)]$, $D(\zeta, \tau) = D_{s,n}$. These solutions were computed in Sect. 2.1.5 outside the UFL and correspond to different values of the longitudinal index n . As we showed in that section, all these additional singlemode solutions have a larger oscillation threshold and hence solution Eq. (81) is the first lasing mode.

Stability of this singlemode solution is analyzed by perturbing the state of the system as

$$F(\zeta, \tau) = F_s + e^{i\phi} \delta F(\zeta, \tau), \quad (82)$$

$$P(\zeta, \tau) = P_s + e^{i\phi} \delta P(\zeta, \tau), \quad (83)$$

$$D(\zeta, \tau) = D_s + \delta D(\zeta, \tau), \quad (84)$$

and linearizing the dynamical equations for the perturbations. The study is facilitated by expressing any perturbation δX in terms of its real (δX_R) and imaginary (δX_I) parts — note that δD is real by definition. The system of equations can be expressed in vector form as

$$\partial_\tau \vec{\delta X} = L \cdot \vec{\delta X}, \quad (85)$$

where $\vec{\delta X} = \text{col}(\delta F_R, \delta P_R, \delta D, \delta F_I, \delta P_I)$ and

$$L = \begin{bmatrix} -\sigma - \partial_\zeta & \sigma A & 0 & 0 & 0 \\ \gamma^{-1} D_s & -\gamma^{-1} & \gamma^{-1} |F_s| & 0 & 0 \\ -\gamma |P_s| & -\gamma |F_s| & -\gamma & 0 & 0 \\ 0 & 0 & 0 & -\sigma - \partial_\zeta & \sigma A \\ 0 & 0 & 0 & \gamma^{-1} D_s & -\gamma^{-1} \end{bmatrix}, \quad (86)$$

with F_s , P_s , and D_s given by Eq. (81).

Because of the linear nature of the system (85), any solution $\vec{\delta X}$ can be calculated as $\vec{\delta X}(\zeta, \tau) = \sum_\lambda \vec{\delta X}_\lambda(\zeta) e^{\lambda\tau}$. On the other hand, given the dependence of L on the spatial coordinate ζ only through the gradient ∂_ζ , any $\vec{\delta X}_\lambda(\zeta)$ can be written as $\vec{\delta X}_\lambda(\zeta) = \sum_\alpha \vec{\delta X}_{\lambda,\alpha} \exp(i\alpha\zeta)$. (Outside the UFL, this ansatz is not valid; see below.) Hence any solution $\vec{\delta X}$ can be finally calculated as

$$\vec{\delta X}(\zeta, \tau) = \sum_{\lambda,\alpha} \vec{\delta X}_{\lambda,\alpha} e^{\lambda\tau + i\alpha\zeta}.$$

Thus the dynamical problem (85) is transformed into the following eigenvalue problem

$$\lambda \overrightarrow{\delta X}_{\lambda, \alpha} = L_{\alpha} \cdot \overrightarrow{\delta X}_{\lambda, \alpha}$$

where L_{α} is given by matrix L with ∂_{ζ} substituted by $i\alpha$. Given the block-diagonal form of L_{α} the characteristic polynomial $\mathcal{P}(\lambda; \alpha)$ that determines the Lyapunov exponents λ is factorized as

$$\mathcal{P}(\lambda; \alpha) = \mathcal{P}_I(\lambda; \alpha) \mathcal{P}_R(\lambda; \alpha), \quad (87)$$

$$\mathcal{P}_I(\lambda; \alpha) = \lambda^2 + (\gamma^{-1} + \sigma + i\alpha) \lambda + i\gamma^{-1}\alpha, \quad (88)$$

$$\mathcal{P}_R(\lambda; \alpha) = \lambda^3 + (\gamma^{-1} + \gamma + \sigma + i\alpha) \lambda^2 + [A + \gamma\sigma + i\alpha(\gamma^{-1} + \gamma)] \lambda + 2\sigma(A - 1) + iA\alpha. \quad (89)$$

These polynomials, equated to zero, allow to determine the dependence $\lambda(\alpha)$ of the eigenvalues on the spatial frequency α of the sidemode perturbation. The boundaries of the unstable domain for the multimode instability correspond to cases where $\text{Re}\lambda(\alpha \neq 0) = 0$ (for $\alpha = 0$ one is considering the well known singlemode, or Lorenz–Haken, laser instability, which is not treated here). The singlemode solution will become unstable against sidemodes of spatial frequency α if $\text{Re}\lambda(\alpha) > 0$.

It is easy to show that \mathcal{P}_I has no roots with $\text{Re}\lambda(\alpha) > 0$ for any α . Only marginally $\lambda(\alpha = 0) = 0$ is always a root. This solution does not entail an instability as it never gets positive real part; in fact that root is merely reflecting the phase arbitrariness of the lasing solution. As \mathcal{P}_I is associated with the subspace formed by $\text{col}(\delta F_I, \delta P_I)$, see Eqs. (85) and (86), and that subspace controls the possible growth of perturbations in phase-quadrature with the lasing mode, one concludes that the RNGHI is not a phase instability but an amplitude instability [29, 30]. This result remains valid outside the uniform field limit, as well as when other factors (inhomogeneous broadening, etc) are included, as far as the resonance condition is maintained. As we discuss below (Sect. 2.2.4), detuning does not have any influence in the stability of class-B lasers, which are our main interest. Nevertheless, in class-A and class-C lasers, detuning has a large influence on the stability properties [41, 43, 57].

Regarding the polynomial \mathcal{P}_R — which, *mutatis mutandi*, governs amplitude instabilities — the boundaries of the multimode instability are found by setting $\lambda = -i\omega$. Upon splitting the thus obtained polynomial (now in ω) into its real and imaginary parts and by equating them to zero one can solve for α and ω as

$$\alpha_{\pm} = \omega_{\pm} \left(1 + \frac{\gamma\sigma}{A - \omega_{\pm}^2} \right), \quad (90)$$

$$\omega_{\pm}^2 = \frac{1}{2} \left[3(A - 1) - \gamma^2 \pm \sqrt{R} \right], \quad (91)$$

$$R = (A - 1)(A - 9) - 6\gamma^2(A - 1) + \gamma^4. \quad (92)$$

The homogeneous solution turns out to be unstable for values of α verifying $|\alpha_-| \leq |\alpha| \leq |\alpha_+|$. This unstable domain has the shape of a tongue in the plane

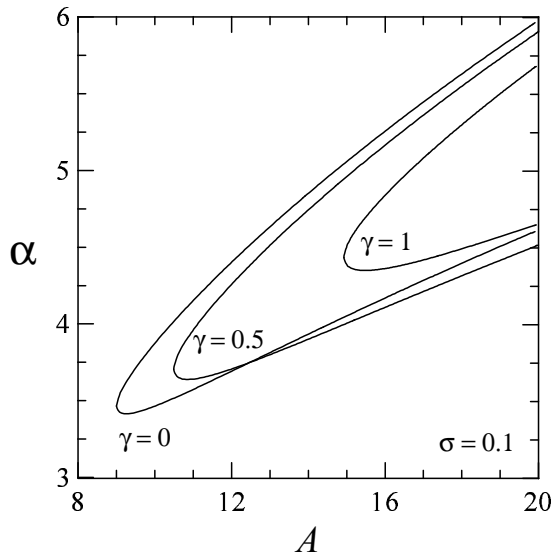


Figure 1: RNGHI threshold in the $\langle r, \alpha \rangle$ plane for the three values of γ marked in the figure.

$\langle A, \alpha \rangle$, and the two branches α_{\pm} merge at the critical point (A_c, α_c) defined by the condition $R = 0$. The critical pump represents the minimum value of A for which the instability can exist, and is given by [29, 30]

$$A_c = 5 + 3\gamma^2 + 4\sqrt{1 + \frac{1}{2}\gamma^2(3 + \gamma^2)}. \quad (93)$$

The value of α_c is obtained from Eqs. (90) and (91) by setting $R = 0$ and $A = A_c$. The results of this linear stability analysis are summarized in Fig. 1.

2.2.2 The RNGH instability in class B lasers

Class B lasers are defined by the inequalities $\gamma_{\parallel} \ll \kappa \ll \gamma_{\perp}$ concerning the decay rates of the population inversion, intracavity field amplitude, and medium polarization, respectively. With the used normalizations those inequalities transform into $\gamma \ll \sigma \ll \gamma^{-1}$. This limit is especially interesting as fiber lasers — and erbium-doped fiber lasers in particular — belong to this class. On the other hand that limit is interesting also from the theoretical viewpoint as it allows to obtain a wealth of analytical information. The latter does not show up in the “classical” version of the RNGHI we have just considered, as the linear stability analysis of the singlemode solution against multimode perturbations is completely analytical. In this section we apply the class B limit to the general expressions already obtained above. In the following section we show how the same results can be derived using asymptotic techniques that employ γ as an expansion parameter.

The expressions for the instability boundaries in the class B limit are retrieved from Eqs. (90)–(92) by setting $\gamma = 0$

$$\alpha_{\pm}^2 = \frac{1}{2} \left[3(A-1) \pm \sqrt{(A-1)(A-9)} \right], \quad (94)$$

$$\omega_{\pm} = \alpha_{\pm}. \quad (95)$$

The critical pump A_c is obtained from Eq. (93) by making $\gamma = 0$ and reads

$$A_c = 9, \quad (96)$$

which is in fact the minimum value A_c can attain. As the first (lasing) threshold occurs at a pump $A = 1$, we conclude that in order to have a RNGHI the pump parameter A should be at least a factor of nine greater than its value at lasing threshold. This is the famous “factor-of-nine”.

As for the sidemode critical frequency α_c , we obtain

$$\alpha_c = \sqrt{12}. \quad (97)$$

So far we have assumed implicitly a continuum of longitudinal modes labelled by their wavenumber offset α . But it must be remembered that the periodic boundary condition (80) imposes, in particular, that the perturbation wavenumber α must be an integer multiple of the scaled cavity free spectral range $\tilde{\alpha}$, Eq. (16)

$$\alpha = \alpha_n = n\tilde{\alpha} = n \frac{2\pi c}{\mathcal{L}_c \sqrt{\gamma_{\parallel} \gamma_{\perp}}}, \quad n \text{ integer}. \quad (98)$$

Thus, in order to have an instability at the lowest possible pump $A = A_c$ the critical frequency α_c must verify (98); alternatively, the cavity (optical) length \mathcal{L}_c must verify

$$\mathcal{L}_c = n \frac{\pi c}{\sqrt{3\gamma_{\parallel} \gamma_{\perp}}}, \quad n \text{ integer}. \quad (99)$$

Hence the shortest cavity length that allows the RNGHI at $A = A_c$ is

$$\mathcal{L}_{c,\min} = \frac{\pi c}{\sqrt{3\gamma_{\parallel} \gamma_{\perp}}}, \quad (100)$$

which is the “critical cavity length” which we referred to in the introduction.

Next we analyze the influence of the actual value of the cavity length (or, alternatively, the consequences on the instability of discrete nature of the cavity modes) on the instability. The analysis will clarify the meaning of $\mathcal{L}_{c,\min}$, which we anticipate is not a true minimum (critical) value for the cavity length, but only the minimum value of \mathcal{L}_c for the instability to occur at the lowest pump. Let us consider the RNGHI boundary, Eq. (94), shown in Fig. 2. Besides the critical point (A_c, α_c) another relevant point is the minimum of α_- vs. A , which is easily determined from Eq. (94) and evaluates to $\alpha_{\min} = 2 + \sqrt{2}$. This quantity is relevant as it settles the minimum frequency of a sideband that can

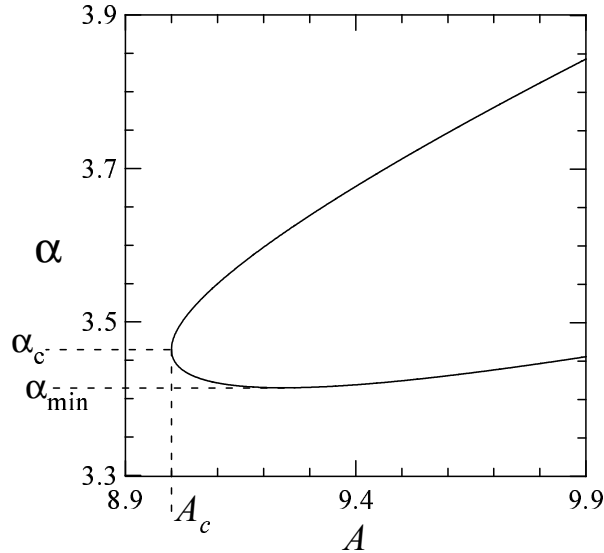


Figure 2: Enlargement of Fig. 1 for $\gamma = 0$.

be linearly amplified after the RNGHI. If the cavity is short in the sense that its free spectral range $\tilde{\alpha}$ is greater than α_{\min} (*i.e.* if $\mathcal{L}_c < \mathcal{L}_* \equiv \frac{2\pi}{2+\sqrt{2}} \frac{c}{\sqrt{\gamma_{\parallel}\gamma_{\perp}}}$) then the sideband with lowest threshold (which we denote by A_{thr}) will be the first one (the one with $\alpha = \tilde{\alpha}$). This threshold value is obtained from Eq. (94) and reads

$$A_{\text{thr}} = \frac{1}{4} \left(2 + 3\alpha^2 - \sqrt{4 - 12\alpha^2 + \alpha^4} \right), \quad (101)$$

where α must be substituted by $\tilde{\alpha}$ and the expression is only valid for $\alpha \geq \alpha_{\min} = 2 + \sqrt{2}$ ⁵. As by decreasing \mathcal{L}_c , $\tilde{\alpha}$ increases, the RNGHI is produced at increasing pump values according to Eq. (101) so that $A_{\text{thr}} \rightarrow \infty$ for $\mathcal{L}_c \rightarrow 0$. This reasoning evidences that $\mathcal{L}_{c,\min}$ is not a true minimum value for the cavity length in order to observe the RNGHI, contrarily to what is commonly believed. Clearly, by lowering \mathcal{L}_c A_{thr} can become so huge that, in practice, the RNGHI can be ruled out. But we stress that this is a practical, not a fundamental, limitation. On the other hand when $\mathcal{L}_c > \mathcal{L}_*$ then $\tilde{\alpha} < \alpha_{\min}$ and the instability is produced at a higher order sideband. The identification of the sideband with lowest threshold is now a more involved task (see [77] for a discussion). In general, for each value of \mathcal{L}_c , A_{thr} must be computed from Eq. (101) by taking $\alpha = n\tilde{\alpha}$ with $n = 1, 2, 3, \dots$ and the lowest value of A_{thr} corresponds to the actual instability threshold value. Fig. 3 displays the actual RNGHI threshold as a function of the cavity length. We note that the graph has periodically recurring minima. This is due to the fact that whenever Eq. (99) is verified, $A_{\text{thr}} = A_c = 9$. All the above analysis can be applied to three- and four-

⁵We note that this equation corrects some typos appearing in Eq. (45) of [77].

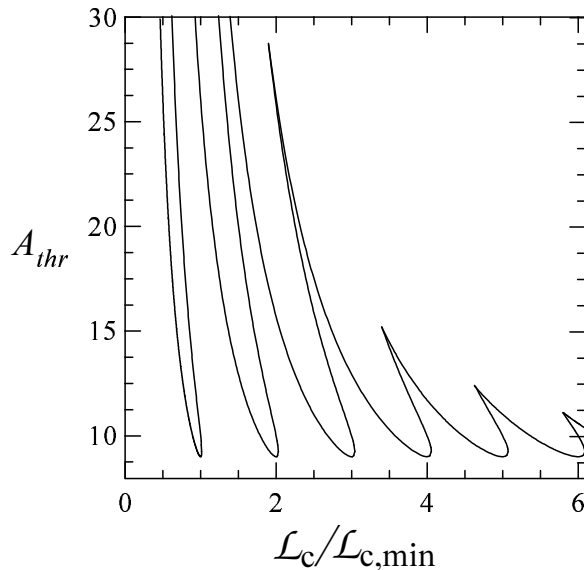


Figure 3: RNGHI threshold as a function of the cavity length for $\gamma = 0$.

level lasers making use of the transformations defined in Sect. 2.1.2: (i) replace A by using Eq. (29), and (ii) replace the spatial frequency α by $\alpha\sqrt{1+W}$ in the final expressions (remember that W is the actual pumping strength). As already advanced in Sect. 2.1.2, for four-level lasers the situation is quite similar to that of two-level lasers, but for three-level lasers the scenario changes dramatically [77] as we discuss next. On the one hand the critical value for two-level lasers $\alpha_c = \sqrt{12}$, Eq. (97), must be replaced by $\sqrt{12(1+W_c)}$ where W_c is the minimum (critical) instability threshold referred to the actual optical pumping W , which is given by

$$W_c = \frac{G+9}{G-9}. \quad (102)$$

Here G is the gain coefficient for three-level lasers defined in Eq. (30). For $G \gg 1$, as is typical in erbium-doped fiber lasers [77], $W_c \rightarrow 1$ and then $\alpha_c^{(3L)} = \sqrt{12(1+W_c)} \rightarrow \sqrt{24}$, which is a factor $\sqrt{2}$ larger than for two-level lasers. With respect to $\mathcal{L}_{c,\min}$

$$\mathcal{L}_{c,\min}^{(3L)} = \frac{\pi c}{\sqrt{6\gamma_{\parallel}\gamma_{\perp}}} \sqrt{\frac{G-9}{G}} \simeq \frac{\pi c}{\sqrt{6\gamma_{\parallel}\gamma_{\perp}}} \quad (103)$$

This value of $\mathcal{L}_{c,\min}$ is $\sqrt{2}$ times smaller than the corresponding two-level value (100). However the most fascinating difference with two-level lasers is the extremely low instability threshold obtained in three-level lasers. Denoting by W_{on}

the lasing threshold referred to W , one has $W_c/W_{\text{on}} \simeq 1 + 16/G$ when $G \gg 1$, as already discussed in Sect. 2.1.2 (see Eq. (32)). Thus in erbium-doped fiber lasers the RNGHI is predicted to occur just above threshold [75, 77]. Finally, the variation of the instability threshold with the cavity length in three-level lasers is much less pronounced than in two-level lasers and, in fact, the cavity can become substantially shorter than $\mathcal{L}_{c,\text{min}}$ while the instability threshold keeps moderate values; see Fig. 6 in [77].

2.2.3 Asymptotic expansions for class B lasers

The results discussed in the previous section have been obtained by applying the class B limit $\gamma \rightarrow 0$ to the general expressions obtained in Sect. 2.2.1, which are valid for arbitrary values of the laser parameters. In other instances (e.g., outside the uniform field limit) this strategy is not possible as general expressions are not available. In such cases one can still obtain a lot of analytical information if the study is done, *ab initio*, for class B lasers. Those treatments rely on asymptotic expansions of the problem that use γ as a smallness parameter. Although in the UFL this analysis is not necessary, we prefer to introduce the technique at this point as here the explanations are more transparent and straightforward than in more complex cases that will be considered below.

The starting point of the analysis is the characteristic polynomial governing the RNGHI, which must be equated to zero in order to obtain the eigenvalues λ that govern the stability of the singlemode lasing solution. In the UFL it is given by Eq. (89), which we recall for convenience

$$\begin{aligned} \mathcal{P}_R(\lambda; \alpha) = & \lambda^3 + (\gamma^{-1} + \gamma + \sigma + i\alpha) \lambda^2 + \\ & [A + \gamma\sigma + i\alpha(\gamma^{-1} + \gamma)] \lambda + 2\sigma(A - 1) + iA\alpha. \end{aligned}$$

(We ignore the polynomial \mathcal{P}_I associated with the phase as we showed it does not contain any instability.) Now, as $0 < \gamma \ll 1$ defines class B lasers (together with $\sigma \sim \gamma^0$), we assume the following ansatz

$$\lambda = \lambda_0 + \gamma\lambda_1 + \gamma^2\lambda_2 + \dots, \quad (104)$$

for the eigenvalues. The ansatz is substituted into $\mathcal{P}_R(\lambda; \alpha)$ and the resulting polynomial is expanded in series of γ as

$$\mathcal{P}_R = \sum_{n=N}^{\infty} \gamma^n p_n(\{\lambda_i\}; \alpha), \quad (105)$$

and, in our case, the expansion (105) starts at $N = -1$.

Now \mathcal{P}_R must be equated to zero. As the expansion is assumed to be uniformly valid for any γ , we impose that each of the p_n be null. Starting at the leading order $n = N (= -1)$, we have

$$p_{-1} = \lambda_0(\lambda_0 + i\alpha),$$

which has the roots

$$\lambda_0 = 0 \quad \text{and} \quad \lambda_0 = -i\alpha. \quad (106)$$

The next order ($n = 0$) reads

$$p_0 = \lambda_0 \lambda_1 + (\lambda_0 + i\alpha) (\lambda_1 + A + \lambda_0^2) + 2\sigma (A - 1) + \sigma \lambda_0^2. \quad (107)$$

Making use of the first root $\lambda_0 = 0$ and equating p_0 to zero we obtain $\lambda_1 = -A + 2i\sigma (A - 1) / \alpha$. As $\text{Re}\lambda_1 < 0$ the roots corresponding to $\lambda_0 = 0$ do not entail an instability and can be discarded. Then we must seek instabilities associated with $\lambda_0 = -i\alpha$, Eq. (106). Substituting this root into Eq. (107) and making $p_0 = 0$, we obtain

$$\lambda_1 = i\sigma\alpha \left[1 - \frac{2}{\alpha^2} (A - 1) \right]. \quad (108)$$

As $\text{Re}\lambda_1 = 0$ we must continue the analysis. At the next order ($n = 1$), once Eqs. (106) and (108) have been used, and after making $p_1 = 0$ we obtain

$$\lambda_2 = -\frac{\sigma}{\alpha^2} [\alpha^4 - 3\alpha^2 (A - 1) + 2A (A - 1)] - i\sigma^2\alpha \left[1 - \frac{4}{\alpha^4} (A - 1)^2 \right]. \quad (109)$$

The analysis can stop here as $\text{Re}\lambda_2$ is not identically zero. The instability boundary $\text{Re}\lambda = 0$ reads in this case $\text{Re}\lambda_2 = 0$, which exactly reduces to the instability boundary for class B lasers Eq. (94), or Eq. (101), as can be checked easily. Regarding the oscillation frequency at the instability threshold, which we denoted by ω in the previous sections, it corresponds to $\text{Im}\lambda$. To the leading order $\text{Im}\lambda = \text{Im}\lambda_0 = -\alpha$, Eq. (106). Thus it is predicted that $\omega = \alpha$, in agreement with Eq. (95).

This kind of analysis will be used later in order to treat more involved problems which, usually, do not admit general analytical expressions to which the class B limit $\gamma \rightarrow 0$ can be applied.

To conclude, we note that the above expansion assumes implicitly that all parameters are of order γ^0 . Obviously, additional scalings can be incorporated if needed, as it occurs in the next section. For instance, in order to fully understand the bifurcation in the presence of inhomogeneous broadening, the scaling $\alpha = \gamma^{-1}\alpha_{-1}$ must be studied separately [81].

2.2.4 Role of detuning in class B lasers

Throughout this paper we shall be dealing with resonant models, as we have just done in the previous sections. Here we prove that detuning between the cavity and the gain line, which is almost unavoidable in real experiments, can be ignored in class B lasers. This is important as it demonstrates that the predictions of resonant models remain valid, to the leading order, even when cavity detuning is present. The analysis will be done in the UFL for the sake of

simplicity. Thus the starting point of the analysis are Eqs. (73)–(75)

$$\begin{aligned}(\partial_\tau + \partial_\zeta)F &= \sigma [AP - (1 - i\Delta)F] , \\ \partial_\tau P &= \gamma^{-1} [FD - (1 + i\Delta)P] , \\ \partial_\tau D &= \gamma [1 - D - \text{Re}(F^*P)] ,\end{aligned}$$

with the boundary condition (76)

$$F(0, \tau) = F(\zeta_m, \tau) , \quad \zeta_m = 2\pi/\tilde{\alpha} .$$

where $\tilde{\alpha}$ is the scaled cavity free spectral range, Eq. (16), and

$$\Delta = \frac{\delta}{1 + \gamma\sigma} . \quad (110)$$

As pointed out in the derivation of the equations in the UFL, by definition $|\delta| \leq \gamma\tilde{\alpha}/2$. In the class B limit $\gamma \ll 1$ and $\sigma = \mathcal{O}(\gamma^0)$, hence $|\Delta| \leq \frac{1}{2}\gamma\tilde{\alpha}$ to the leading order. Next we determine the maximum admissible order of magnitude of Δ . For that we note, based on the results of the resonant model discussed in the previous sections, that $\tilde{\alpha}$ must be at most a quantity of order γ^0 for the instability to occur at physically realizable pumping levels. Hence Δ is, at most, of order γ . This is shown by the following argument: As the case of small $\tilde{\alpha}$ (say $\tilde{\alpha} \sim \gamma^k$ with $k = 1, 2, \dots$) poses no problem (in this case Δ would be still smaller) we concentrate on the large free spectral range limit $\tilde{\alpha} \gg 1$. In this case, as discussed in Sect. 2.2.2, the first sideband ($\alpha = \tilde{\alpha}$) is the one with lowest instability threshold, whose value is given by Eq. (101). The asymptotic form of such equation in the limit $\tilde{\alpha} \gg 1$ reads

$$A_{\text{thr}} \xrightarrow{\tilde{\alpha} \gg 1} \frac{1}{2}\tilde{\alpha}^2 .$$

Then, if $\tilde{\alpha} \sim \gamma^{-1}$, $A_{\text{thr}} \sim \gamma^{-2} \sim 10^{10}$ (for typical fiber lasers $\gamma \sim 10^{-5}$), and this is nonsense⁶. The conclusion is that, unless completely unrealistic pumping values are considered, $\tilde{\alpha}$ must be a quantity of order γ^0 (at most) and then an appropriate scaling for class B lasers is $\Delta = \gamma\Delta_1$, with Δ_1 of order γ^0 .

The singlemode solution with lowest threshold is the stationary solution given by Eq. (62), that we recall here for convenience

$$F_s = \sqrt{A - 1 - \Delta^2} e^{i\phi} , \quad P_s = \frac{F_s}{A} (1 - i\Delta) , \quad D_s = \frac{1 + \Delta^2}{A} .$$

For $\Delta = 0$ this solution reduces to the resonant singlemode solution (81) analyzed in the previous sections. The lasing threshold $1 + \Delta^2$ differ from that of a perfectly resonant laser only by a term of order γ^2 as Δ is of order γ .

The stability of the stationary solution can be studied as in Sect. 2.2.1. In this case however, the presence of the atomic detuning Δ introduces an

⁶Even for a moderate value as $\tilde{\alpha} = 20$ (which is still of order γ^0), the actual instability threshold is $A_{\text{thr}} = 202.01$, which is clearly a huge pumping ratio.

entanglement between the real and imaginary parts of the fluctuations, and the fifth order characteristic polynomial cannot be any longer factorized as in the resonant case, Eq. (87). The analysis of the eigenvalues is much more complicated and it is convenient to apply the asymptotic expansion presented in Sect. 2.2.3. We do not give the details of the derivation, which is straightforward but lengthy. We just want to emphasize that the relevant eigenvalue obtained in this way reads $\lambda = -i\alpha + \gamma\lambda_1 + \gamma^2\lambda_2 + O(\gamma^3)$, where λ_1 and λ_2 are the very same we obtained in the resonant case analyzed in Sect. 2.2.3. In particular this means that the detuning $\Delta = \gamma\Delta_1$ does not have any influence to the leading order (probably it appears at corrections of order γ^3 or smaller, but these do not control the instability). The conclusion is then clear: In class B lasers the influence of the cavity detuning does not show up to the leading order. Then one can safely ignore that detuning and the results obtained in resonant models can be considered as an excellent approximation to detuned models.

2.2.5 Spatial effects

When the plane-wave approximation is abandoned and one assumes, more realistically, that the laser operates on the fundamental Gaussian mode (TEM_{00}), the RNGHI (as well as the Lorenz–Haken instability) turns out to be strongly influenced by the relative size of the beam and the amplifying medium. If r_m is the radius of the amplifying medium and w_0 the beam waist, the relevant parameter is $u_m = 2(r_m/w_0)^2$. In two-level lasers it was demonstrated that the instability disappears in the limit $u_m \gg 1$ [82, 83, 84], but it is recovered as soon as u_m becomes of order unity [85, 86]. This result can be easily understood considering that in the limit $u_m \ll 1$ of very narrow amplifying medium the model equations for a Gaussian beam reduce to those of the plane-wave approximation, because the wavefront can be assumed to be plane inside the amplifying medium. The results of [86] apply well to fibre lasers, where the dopant is usually confined inside the fibre core, whose radius r_{core} is typically smaller than the waist of the laser beam. Yet, we know that when considering fibre lasers one must distinguish between three- and four-level atoms, because of the different dependence on the pump of the equilibrium population difference d_0 .

The Maxwell-Bloch equations for a Gaussian beam in three- and four-level lasers are Eqs. (42–44), derived in Sect. 2.1.3. Here we limit our analysis to the UFL. Following the same steps as in Sect. 2.1.5, it can be easily shown that the Maxwell-Bloch equations in the resonant case in the UFL are [79, 87]

$$(\partial_\tau + \partial_\zeta) F = \sigma \left[G \int_0^{u_m} du e^{-u/2} P - F \right]. \quad (111)$$

$$\partial_\tau P = \gamma^{-1} \left(e^{-u/2} F D - P \right), \quad (112)$$

$$\partial_\tau D = \gamma \left[\beta e^{-\eta u} (1 - D) - \delta_{N,3} - D - e^{-u/2} F P \right]. \quad (113)$$

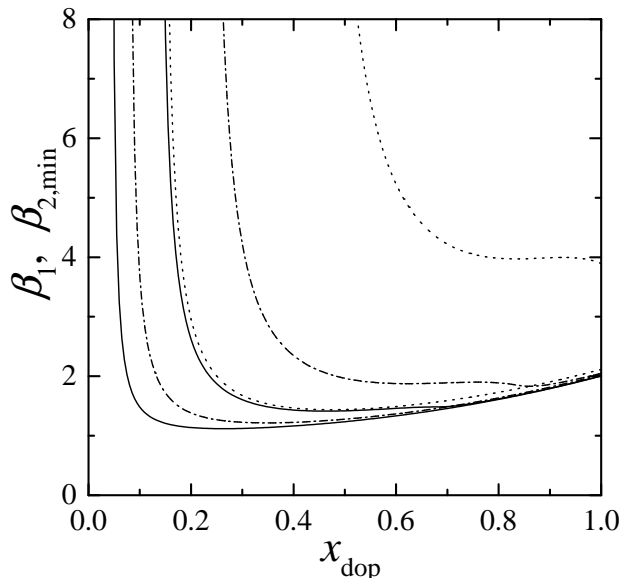


Figure 4: Lasing threshold β_1 and minimum instability threshold $\beta_{2,min}$ as functions of the scaled radius of the doped region x_{dop} for three values of the gain parameter G : $G = 600$ (solid lines), $G = 200$ (dashed–dotted lines) and $G = 60$ (dotted lines). For each value of G the singlemode solution exists and is stable in the region between the two lines.

with the periodic boundary condition

$$F(0, u, \tau) = F(\zeta_m, u, \tau), \quad \zeta_m = 2\pi/\tilde{\alpha}. \quad (114)$$

Here we assumed without loss of generality that both F and P are real. We recall that β is the intensity of the pump field, and the parameter η is defined as $\eta = (w_0/w_p)^2$, where w_p is the waist of the pump beam. The parameter $\delta_{N,3}$, which is equal to 1 for three–level lasers and to 0 for four–level lasers, makes the difference between the two situations.

Transverse effects in Erbium–doped (three–level) fibre lasers were investigated in [87]. It was assumed that the dopant is confined inside the core of the fibre, *i.e.* $r_m \leq r_{core}$. The ratio

$$x_{dop} = \frac{r_m}{r_{core}} \quad (115)$$

was used as a free parameter, ranging 0 to 1. For fibre lasers of the type used in [72] adequate parameters are $w_p = 2.086 \mu\text{m}$ and $w_0 = 2.828 \mu\text{m}$, which implies $\eta = 1.839$, and $r_{core} = 1.875 \mu\text{m}$ [72, 76]. Since u_m can be written as $u_m = 2(r_{core}/w_0)^2 x_{dop}^2$, with our parameters we have $u_m = 0.879 x_{dop}^2$. The proper pump parameter now is the pump intensity β . We call β_1 the

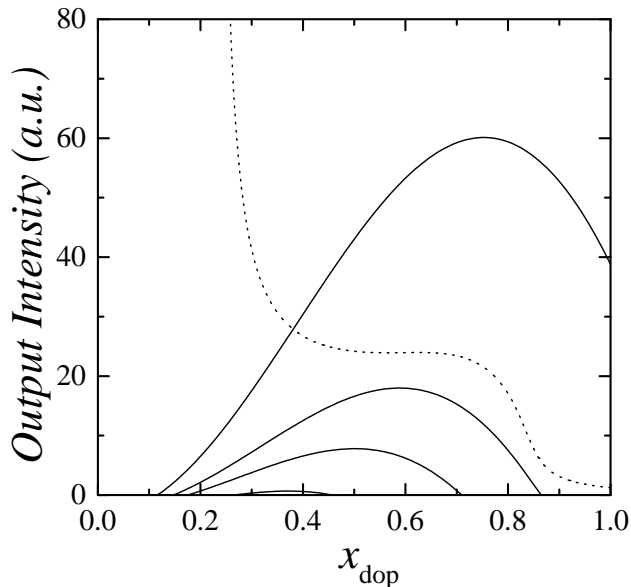


Figure 5: Solid lines: output intensity as a function of the scaled radius of the doped region x_{dop} for $G = 200$ and for different values of the pump intensity, $\beta = 1.25, 1.5, 1.75, 2.5$ from bottom to top. Dashed line: output intensity in correspondence of the minimum instability threshold $\beta_{2,\text{min}}$.

lasing threshold and β_2 the threshold for the RNGHI. The minimum instability threshold, which is the one corresponding to the critical frequency space α_c where the upper and lower instability boundaries merge, is denoted by $\beta_{2,\text{min}}$.

A first important result is shown in Fig. 4, where the dependence of β_1 and $\beta_{2,\text{min}}$ on the normalized doped radius x_{dop} is shown for three experimentally accessible values of the gain parameter G . All curves display a vertical asymptote for small doped regions, and it may be noted that, for each value of G , the asymptote for $\beta_{2,\text{min}}$ corresponds to a value of x_{dop} which is about three times larger than the one associated with the asymptote for β_1 . The existence of these asymptotes can be explained making reference to the plane-wave limit, to which the model reduces in the limit $x_{\text{dop}} \rightarrow 0$ (which implies $u_m \rightarrow 0$) [87]. It can be shown that the two asymptotes are well approximated by $x_{\text{dop}} = 1/\sqrt{0.879G}$ and $x_{\text{dop}} = 3/\sqrt{0.879G}$, where the factor 0.879 comes from $u_m = 0.879 x_{\text{dop}}^2$.

Thus, there exists a band of values of x_{dop} between the two asymptotes, where singlemode lasing is stable for all pump strengths. One is tempted to conclude that to stabilize the laser it suffices to dope only a small fraction of the fibre core. But Fig. 4 also tells us that the lasing threshold β_1 rapidly increases for small x_{dop} , which means that, for a given pump β , the output intensity decreases. A compromise between stability and not too low output

intensity must be found.

Fig. 5 shows how the output intensity I depends on x_{dop} for four increasing values of the pump intensity β , and $G = 200$. All curves are similar and display a maximum that shifts to larger doped area radii as β increases. Also displayed, as a dashed line, is the critical intensity $I_{2,\text{min}}$ associated with the minimum instability threshold $\beta_{2,\text{min}}$. All stationary intensities in Fig. 5 which are above $I_{2,\text{min}}$ are unstable (multimode emission takes place). We show only the case $G = 200$ for the sake of clarity. The vertical asymptote of $I_{2,\text{min}}$ corresponds to that of $\beta_{2,\text{min}}$ in Fig. 4 for $G = 200$. Interestingly, $I_{2,\text{min}}$ shows a relatively large plateau for $0.4 \leq x_{\text{dop}} \leq 0.7$. In this region the maximum stable singlemode intensity available is almost insensitive to x_{dop} , what constitutes a genuine transverse effect, not explainable in the plane-wave limit.

The best operating conditions are given by an interplay between plane-wave limit and transverse effects. In the particular case considered ($G = 200$), the plane-wave limit indicates that stable singlemode emission is guaranteed if $0.1 \leq x_{\text{dop}} \leq 0.25$, but in this region very large values of the pump intensity are required in order to obtain a large output intensity. However, the particular dependence of the output intensity on x_{dop} , which is a consequence of the transverse profile of the laser and pump beams, shows that stable emission with sufficiently high intensity can be achieved for smaller pump intensities when the radius of the doped area is larger ($x_{\text{dop}} \simeq 0.6$).

A similar analysis was performed in Ref. [79] for a ring Nd:YAG (four-level) laser using Eqs. (111–113) with $\delta_{N,3} = 0$. At difference with the erbium-doped fiber laser, in the case of a bulk Nd:YAG laser the dopant distribution can be assumed to be homogeneous, and to some approximation the same holds for the pump (at least in side-pumped designs). Then, the only transverse effects that have to be taken into account are the Gaussian profile of the laser field and the finite dimension of the active medium (the laser rod). In [79] it was demonstrated that the instability occurs whenever the beam waist w_0 is slightly larger, or at least equal to r_m , the radius of the active medium's rod. To accomplish this is not a trivial task, as it is discussed in detail in [79], but it seems feasible with present day technology. As Nd is a four-level medium, in this case the instability to lasing threshold ratio is slightly larger than 9 in the optimal conditions (see Sect. 2.1.2), *i.e.*, in this case the instability threshold is well separated from the lasing one. We refer the reader to [79] for full details.

2.3 Outside the uniform field limit

The study of lasers instabilities outside the uniform field limit is in general a difficult task, because even the stationary state is spatially dependent [58]. But the best candidates for the observation of the RNGHI are fibre lasers, for which the UFL usually does not apply, because the effective reflectivity parameter \mathcal{R} is far from unity. On the other hand, these lasers satisfy very well the class-B limit, because the parameter γ is as small as 10^{-5} [72, 77, 88, 89]. This is a fortunate circumstance because, as we shall show in the present section, at least in the study of the RNGHI, the class-B limit is as powerful as the UFL, in

the sense that the analytical results obtained in the UFL can be generalized to arbitrary \mathcal{R} in class-B lasers.

Specifically, in this section we will show that for class-B lasers outside the UFL the following results hold: (i) the boundaries of the stability domain of the homogeneous solution can be determined analytically, (ii) the simple self-pulsing solutions can be studied in a completely analytic way, (iii) the multimode dynamics arising from the instability can be described in terms of a limited number of Fourier modes. In all cases cavity detuning will be ignored after the discussion in Sect. 2.2.4.

This section is organized as follows: In Sect. 2.3.1 we derive the RNGHI outside the UFL. Then we generalize the result by taking into account distributed losses (Sect. 2.3.2). In Sect. 2.3.3 we derive generalized rate equations for class-B lasers, and in Sect. 2.3.4 we use those equations to analyze self-pulsing. In Sect. 2.3.5 we discuss the issue of the numerical integration of the model and present some numerical results in order to compare the different integration methods. Finally, in Sect. 2.3.6 we address the issue of the super- or sub-criticality of the bifurcation.

2.3.1 RNGH outside the UFL

First we consider the case when no distributed losses exist in the laser cavity ($\chi = 0$) and recall the Maxwell-Bloch equations (18)–(20) valid in the resonant case

$$(\partial_\tau + \partial_\zeta) F = \sigma AP, \quad (116)$$

$$\partial_\tau P = \gamma^{-1} (FD - P), \quad (117)$$

$$\partial_\tau D = \gamma (1 - D - FP), \quad (118)$$

together with the boundary condition

$$F(0, \tau) = \mathcal{R}F(\zeta_m, \tau), \quad \zeta_m = 2\pi/\tilde{\alpha}, \quad (119)$$

where $\zeta = 0$ and $\zeta = \zeta_m$ denote the location of the entry and exit faces of the active medium, and $\tilde{\alpha}$ is the scaled cavity free spectral range, Eq. (16).

In these equations we have assumed that the fields F and P are real because we showed in Sect. 2.2.1 that in the resonant case and in the UFL, the RNGHI is an amplitude instability. Lifting the UFL does not change the nature of the bifurcation, as can be checked following the lines of our study in Sect. 2.2.1.

Unlike in the UFL, now all variables at steady state are in general functions of the coordinate ζ , as we showed in Section 2.1.4. According to Eq. (54) the steady value of the field intensity $I_s = |F_s|^2$ at the medium exit face is given by

$$I_s(\zeta_m) = \frac{|\ln \mathcal{R}^2|}{1 - \mathcal{R}^2} (A - 1), \quad (120)$$

and $A = 1$ corresponds to the first laser threshold.

As in previous sections, the linear stability analysis is performed by writing $F(\zeta, \tau) = F_s(\zeta) + \delta F(\zeta) \exp(\lambda\tau)$, and similar expressions for P and D , and

linearizing the resulting dynamical equations. As now the problem depends explicitly on the longitudinal coordinate ζ and the boundary condition is not periodic, one cannot make the ansatz $\delta F \sim \exp(i\alpha\zeta)$ as in the UFL. In fact, now the spatial dependence of δF is unknown a priori and an equation for it must be sought. After solving for the material perturbations we set $\delta F(\zeta) = F_s(\zeta)\delta f(\zeta)$ and obtain the following equation for δf

$$\begin{aligned}\frac{d}{d\zeta}\delta f &= -\lambda\delta f - H(I_s)\delta f, \\ H(I_s) &= \frac{\sigma A}{1+I_s} \frac{\gamma\lambda(\lambda+\gamma) + 2\gamma I_s}{(\gamma+\lambda)(1+\gamma\lambda) + \gamma I_s},\end{aligned}$$

whose formal integration yields

$$\begin{aligned}\delta f(\zeta) &= \delta f(0) \exp[-\lambda\zeta - \psi(\zeta)], \\ \psi(\zeta) &= \int_0^\zeta d\zeta' H(I_s(\zeta')).\end{aligned}$$

The evaluation of the integral $\psi(\zeta)$ requires a change of variable from ζ to I_s [46] through the steady state equation $dI_s/d\zeta = 2\sigma AI_s/(1+I_s)$, after which the following result is obtained [90]

$$\psi(\zeta) = \frac{\gamma\lambda}{2(1+\gamma\lambda)} \ln \frac{I_s(\zeta)}{I_s(0)} + \frac{2+\gamma\lambda}{2(1+\gamma\lambda)} \ln \frac{(1+\gamma\lambda)(\lambda+\gamma) + \gamma I_s(\zeta)}{(1+\gamma\lambda)(\lambda+\gamma) + \gamma I_s(0)}. \quad (121)$$

Finally we return to the initial perturbation $\delta F(\zeta)$ and write

$$\delta F(\zeta) = \delta F(0) \frac{F_s(\zeta)}{F_s(0)} \exp[-\lambda\zeta - \psi(\zeta)]. \quad (122)$$

The boundary condition (119) applied to the perturbation $\delta F(\zeta)$ gives the following characteristic equation

$$\lambda = -in\tilde{\alpha} - \frac{\psi(\zeta_m)}{\zeta_m}, \quad (123)$$

where Eq. (22) has been used. Recalling (119) and making use of the steady intensity Eq. (120), the function $\psi(\zeta_m)$ reads

$$\begin{aligned}\psi(\zeta_m) &= \frac{\gamma\lambda}{2(1+\gamma\lambda)} |\ln \mathcal{R}^2| + \frac{2+\gamma\lambda}{2(1+\gamma\lambda)} \\ &\times \ln \left[1 + \frac{\gamma |\ln \mathcal{R}^2| (A-1)}{(1+\gamma\lambda)(\lambda+\gamma) + \gamma \frac{\mathcal{R}^2 |\ln \mathcal{R}^2|}{1-\mathcal{R}^2} (A-1)} \right].\end{aligned} \quad (124)$$

Equation (123) is the characteristic equation governing the eigenvalues λ . It is a transcendental equation in λ and hence no explicit expressions can be obtained. However in the class B limit $\gamma \rightarrow 0$, the use of an asymptotic expansion of (123)

in powers of γ similar to that introduced in Sect. 2.2.3 allows to completely unfold the problem. After writing $\lambda = \lambda_0 + \gamma\lambda_1 + \gamma^2\lambda_2 + \dots$ one obtains [90]

$$\begin{aligned}\lambda_0 &= -i\alpha, \\ \lambda_1 &= i\sigma\alpha \left[1 - \frac{2}{\alpha^2}(A-1) \right], \\ \text{Re}\lambda_2 &= -\frac{\sigma}{\alpha^2} \left\{ \alpha^4 - 3\alpha^2(A-1) + 2(A-1) \left[1 + \frac{A-1}{2} \frac{1+\mathcal{R}^2}{1-\mathcal{R}^2} |\ln \mathcal{R}^2| \right] \right\}, \\ \text{Im}\lambda_2 &= -\sigma^2\alpha \left[1 - \frac{4}{\alpha^4}(A-1)^2 \right],\end{aligned}$$

where $\alpha = n\tilde{\alpha}$. The RNGHI occurs at $\text{Re}\lambda_2 = 0$, which defines the following boundaries

$$\alpha_{\pm}^2 = \frac{1}{2} \left[3(A-1) \pm \sqrt{(A-1)^2 \mathcal{D} - 8(A-1)} \right], \quad (125)$$

$$\mathcal{D} = 9 - 4 \frac{1+\mathcal{R}^2}{1-\mathcal{R}^2} |\ln \mathcal{R}^2|. \quad (126)$$

Notice the formal similarity with Eq. (94) corresponding to the UFL (for $\mathcal{R} \rightarrow 1$, $\mathcal{D} \rightarrow 1$ and then Eq. (94) is recovered). Now the two curves join at the critical point

$$A_c = 1 + \frac{8}{\mathcal{D}}, \quad (127)$$

$$\alpha_c^2 = \frac{12}{\mathcal{D}}. \quad (128)$$

The boundaries of the unstable domain depend on the reflectivity \mathcal{R} through the function \mathcal{D} . In the UFL $\mathcal{T} \equiv 1 - \mathcal{R}^2 \rightarrow 0$ (\mathcal{T} denotes the fraction of intracavity power lost per roundtrip), \mathcal{D} can be approximated as $\mathcal{D} = 1 - 2(\mathcal{T}^2 + \mathcal{T}^3)/3 + \mathcal{O}(\mathcal{T}^4)$ and therefore the expressions for A_c and α_c become

$$\begin{aligned}A_c &= 9 + \frac{16}{3}\mathcal{T}^2(1+\mathcal{T}) + \mathcal{O}(\mathcal{T}^4), \\ \alpha_c^2 &= 12 + 8\mathcal{T}^2(1+\mathcal{T}) + \mathcal{O}(\mathcal{T}^4).\end{aligned}$$

Both quantities reduce for $\mathcal{T} = 0$ to the ones found in the UFL, namely $A_c = 9$ and $\alpha_c^2 = 12$. Clearly Eq. (125) is meaningful only if the argument of the square root is non-negative, and this requires $\mathcal{D} > 0$ or, equivalently, that the reflectivity must be greater than

$$\mathcal{R}_{\min} \simeq 0.5379. \quad (129)$$

This is an outstanding result as it sets an absolute minimum value to \mathcal{R} in order to observe the RNGHI [90] (see also [36]). In other words, no matter how large the pump or how long the cavity be, the laser will not display multimode

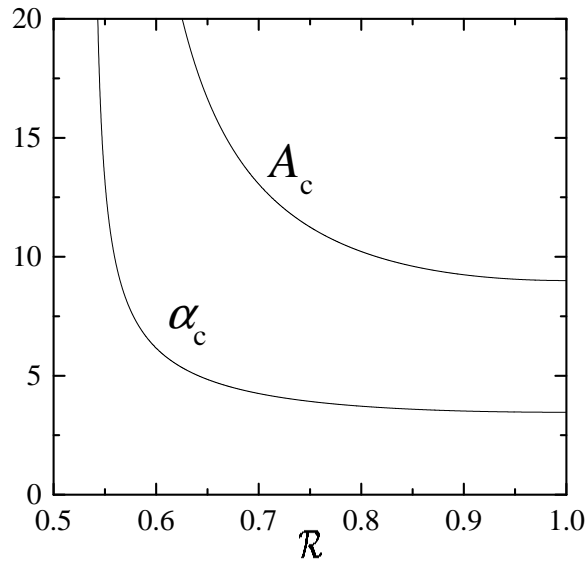


Figure 6: Behavior of the critical values A_c and α_c as functions of the reflectivity \mathcal{R} .

instabilities if $\mathcal{R} < \mathcal{R}_{\min}$. Above this reflectivity value, the effect of lowering \mathcal{R} from the UFL ($\mathcal{R} \rightarrow 1$) is monotonous: Fig. 6 shows that the critical values (A_c, α_c) grow by decreasing \mathcal{R} and diverge by approaching \mathcal{R}_{\min} . Accordingly, as shown in Fig. 7, the instability tongue (125) shifts towards larger pumps and larger wavenumbers.

To conclude, let us remark that unlike in the UFL now the value of cavity loss influences the second-to-first threshold ratio through \mathcal{R} . In the UFL cavity loss affects the pump values necessary for lasing and for instability, but not their ratio. This fact marks a way for separating experimentally the two thresholds in erbium-doped fiber lasers (remember that for these lasers $W_c/W_{\text{on}} = 1 + \epsilon$ in the UFL, i.e. for small cavity losses, rendering the observation of the instability difficult). This is the strategy followed in the experiments [88, 89], which are treated in detail in Sect. 4.

2.3.2 Role of distributed losses

Another factor present in almost any experiment and not considered by the standard RNGH theory is the existence of distributed losses along the amplifying medium, apart from those localized outside it. The two types of losses should have different consequences as the role of distributed loss should be to decrease gain, while localized loss determines the effective reflectivity value \mathcal{R} , whose influence has been studied above. An analysis of the combined effects of distributed and localized losses can be found in Ref. [78], which we summarize

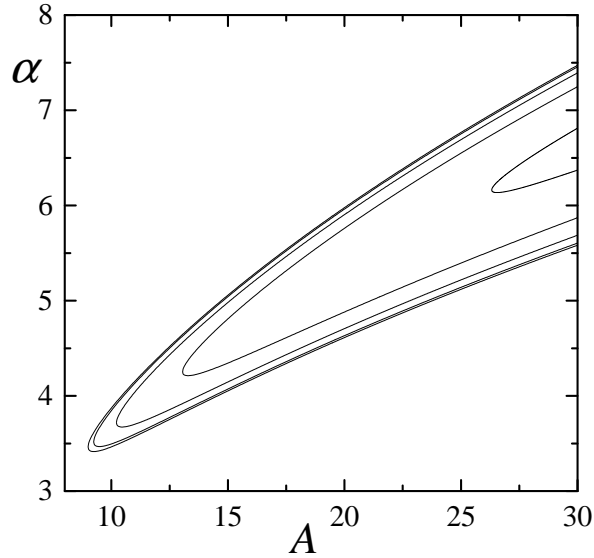


Figure 7: Unstable domains for five different values of the reflectivity \mathcal{R} . From left to right $\mathcal{R} = 0.99$ (which corresponds to the UFL), 0.9, 0.8, 0.7, 0.6.

here. The proper model reads now, Eqs. (18)–(20),

$$(\partial_\tau + \partial_\zeta) F = \sigma (AP - \chi F), \quad (130)$$

$$\partial_\tau P = \gamma^{-1} (FD - P), \quad (131)$$

$$\partial_\tau D = \gamma [1 - D - \text{Re}(F^* P)], \quad (132)$$

where we have ignored again detuning, with the boundary condition

$$F(0, \tau) = \mathcal{R}F(\zeta_m, \tau), \quad \zeta_m = 2\pi/\tilde{\alpha}. \quad (133)$$

The parameter $\chi = \alpha_m L_m / (|\ln \mathcal{R}^2| + \alpha_m L_m)$, Eq. (14), verifies $0 \leq \chi \leq 1$, and α_m is an intensity loss coefficient per unit length⁷.

The intensity of the singlemode solution along ζ , and its value at the medium exit plane are given, respectively, by Eq. (52) and Eq. (53) with $\Delta = 0$, and the lasing threshold is $A = 1$. The linear stability analysis of the singlemode solution follows the lines of the previous sections. As shown in [78] the main effect of distributed loss is to favor the multimode instability, i.e., to reduce the instability to lasing threshold ratio (of course, the larger the losses the larger the pump needed for reaching both the lasing and instability thresholds). For instance, the minimum reflectivity value allowing the existence of the RNGHI,

⁷We note that in Ref. [78] the parameter χ was denoted by η . Another relevant parameter used there, γ_d , can be written as $\gamma_d = \frac{1}{2} |\ln \mathcal{R}^2| \frac{\chi}{1-\chi} = \frac{1}{2} \alpha_m L_m$. The pump parameter A keeps the same definition as in [78].

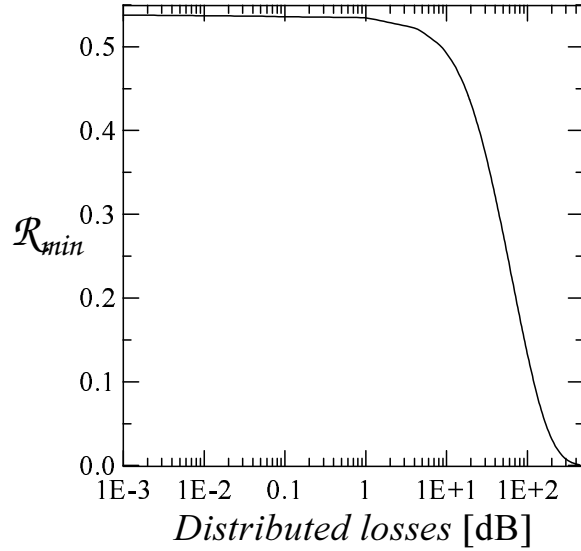


Figure 8: Dependence of the minimum reflectivity necessary for the appearance of the RNGHI as a function of distributed losses expressed in dB.

\mathcal{R}_{\min} , is determined by the equation

$$\frac{8(1-\chi)}{\chi(8-9\chi)} \frac{1-\mathcal{R}^2}{|\ln \mathcal{R}^2|} \frac{1-\exp\left(-\frac{\chi}{1-\chi} |\ln \mathcal{R}^2|\right)}{1-\mathcal{R}^2 \exp\left(-\frac{\chi}{1-\chi} |\ln \mathcal{R}^2|\right)} = 1, \quad (134)$$

which can be simplified to

$$\frac{8}{8-9\chi} \frac{1-\mathcal{R}^2}{\alpha_m L_m} \frac{1-e^{-\alpha_m L_m}}{1-\mathcal{R}^2 e^{-\alpha_m L_m}} = 1. \quad (135)$$

This equation yields $\mathcal{R}_{\min} \simeq 0.5379$ for $\chi = 0$, Eq. (129), as it should. For nonzero distributed loss, \mathcal{R}_{\min} is found to decrease with increasing $\alpha_m L_m$ so that for $\alpha_m L_m \approx 13.6$, $\mathcal{R}_{\min} \simeq 0.1$, and for larger values of $\alpha_m L_m$, $\mathcal{R}_{\min} \rightarrow 0$ exponentially, as shown in Fig. 8. In that figure distributed losses are expressed in decibels (dB) through the relation

$$DL = 8.646 \alpha_m L_m. \quad (136)$$

We can conclude that for $DL < 1$ dB (which is the usual situation), \mathcal{R}_{\min} changes very little, and only for $DL > 10$ dB \mathcal{R}_{\min} decreases very quickly. However, 10 dB is an enormous amount of distributed loss, hardly realistic for a usual laser. So it can safely be said that distributed losses for realistic laser parameters do not significantly affect the multimode emission threshold. An

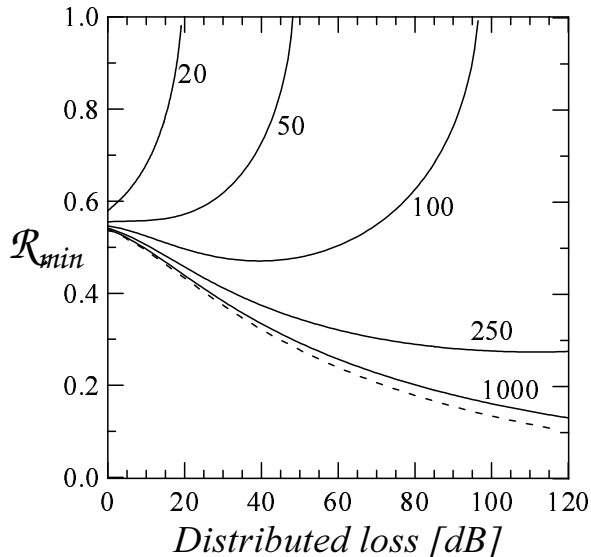


Figure 9: Dependence on distributed losses of the minimum reflectivity necessary for the RNGHI to exist for three-level lasers. The numbers indicate the value of G_0 and the dashed line corresponds to $G_0 \rightarrow \infty$.

important question is whether this conclusion can be extended to three- and four-level lasers: The answer is that it cannot. For example, Eq. (135) is only valid for two-level lasers, i.e., it cannot be directly translated for three- and four-level lasers (this is due to the way it is derived, see the discussion in [78]). When \mathcal{R}_{\min} is calculated for three-level lasers, the result is that of Fig. 9, which tends to the two-level laser result only for very large G .

In general, although the effect of distributed losses can be neglected for two-level lasers, as discussed above, this will not be so for three- and four-level lasers. The origin of this different behavior lays in the fact that distributed losses enter into the definition of the pump parameter, Eq. (13), through G , Eq. (30). Nevertheless, the analysis we carried out for two-level lasers leads to a simplified way of treating distributed loss, as long as it is not too large (roughly, smaller than 10 dB): Perform the linear stability analysis without taking distributed loss into account (which is accurate for two-level lasers), and then take distributed loss into account when translating the results derived for two-level lasers into three- and four-level lasers through G , Eq. (30). We have checked that this is a very accurate way of deriving the stability properties for three- and four-level lasers for not too large distributed loss. We shall make use of this simplified way of treating distributed losses in Sect. 3.3 when inhomogeneous broadening be included

2.3.3 Rate equations

Class-B lasers are usually treated with rate equations, which are derived by equating to zero the time derivative of the medium polarization. If this is done in Eqs. (18–20), then the RNGHI is lost. This means that in order to capture the RNGH instability, coherent effects (*i.e.*, those due to the atomic polarization) must be preserved in the equations: The standard adiabatic elimination technique fails in this case.

Nevertheless, the above circumstance does not prevent the derivation of generalized rate equations that maintain enough information on the medium polarization dynamics as for correctly describing the RNGHI. This is what we do in this section: We derive a reduced set of rate equations, in which the polarization variable is adiabatically eliminated in a generalized sense [91]. The derivation of these equations stems from the observation that the RNGHI instability can be captured only if in the stability analysis terms up to order γ^2 are kept. Therefore, the instability certainly disappears if the rate equations are derived by means of a standard adiabatic elimination of the polarization, which amounts to truncate the polarization to the term of order γ^0 . But with a more refined adiabatic elimination, where terms up to order γ^2 are kept in the polarization, we can derive a set of generalized rate equations that describe perfectly the RNGHI.

To derive the rate equations we start from Eqs. (68–70) introduced in Sect. 2.1.5 for the primed variables F' , P' and D' . The most noticeable property of those equations is that, although they are valid outside the UFL, they admit as a stationary solution the singlemode solution of the UFL (62). In the following we will consider power expansions of the dynamical variables in terms of the small parameter γ . To this aim it is convenient to work with variables which, at the leading order, are of order 1. Therefore, we introduce the new dynamical variables f , p and d defined as

$$f(\zeta, \tau) = \frac{F'(\zeta, \tau)}{\sqrt{I_s^{\text{UFL}}}}, \quad p(\zeta, \tau) = \frac{AP'(\zeta, \tau)}{\sqrt{I_s^{\text{UFL}}}}, \quad d(\zeta, \tau) = AD'(\zeta, \tau). \quad (137)$$

The Maxwell–Bloch equations for f , p and d obtained from Eqs. (68)–(70) are

$$(\partial_\tau + \partial_\zeta) f = \sigma\eta(\zeta) [p - (1 - i\Delta) f], \quad (138)$$

$$\partial_\tau p = \gamma^{-1} [fd - (1 + i\Delta) p], \quad (139)$$

$$\partial_\tau d = \gamma \{1 + \Delta^2 - d + I_s(\zeta) [1 - \text{Re}(f^*p)]\}, \quad (140)$$

The new electric field f obeys the same periodic boundary condition as F'

$$f(0, \tau) = f(\zeta_m, \tau). \quad (141)$$

and in the stationary state it is not only uniform but equal to 1. In fact, Eqs. (138)–(140) admit the stationary solution $f_s = 1$, $p_s = 1 - i\Delta$, $d_s = 1 + \Delta^2$. For

a perfect resonant laser ($\Delta = 0$) they reduce to

$$(\partial_\tau + \partial_\zeta)f = \sigma\eta(\zeta)(p - f), \quad (142)$$

$$\partial_\tau p = \gamma^{-1}(fd - p), \quad (143)$$

$$\partial_\tau d = \gamma \{1 - d + I_s(\zeta) [1 - \text{Re}(f^*p)]\}, \quad (144)$$

and the stationary solution is $f_s = p_s = d_s = 1$. To obtain the correct rate equations we first observe that, by setting $\gamma = 0$ in Eqs. (142–144), we obtain: (i) $\partial_\tau d = 0$, hence $d(\zeta, \tau) = d_0(\zeta)$, (ii) $p = d_0(\zeta)f$, and (iii) $(\partial_\tau + \partial_\zeta)f = \sigma\eta(\zeta)[d_0(\zeta) - 1]f$. Note that these equations do not fix the value of $d_0(\zeta)$. However, since it is independent of time, it must be compatible, in particular, with the stationary solution $d = 1$, which implies $d_0(\zeta) = 1$. Hence, at order 0 in γ we have $d = 1$ and $f = p$, from which it follows that $\partial_\tau f = -\partial_\zeta f$. For $\gamma \neq 0$ we make the following ansatz

$$p = f + \mathcal{O}(\gamma), \quad d = 1 + \mathcal{O}(\gamma), \quad \partial_\tau f = -\partial_\zeta f + \mathcal{O}(\gamma). \quad (145)$$

We now observe that Eq. (143) can be written as $p = fd - \gamma\partial_\tau p$, which, iterated twice, yields

$$p = fd - \gamma\partial_\tau(fd) + \gamma^2\partial_{\tau\tau}^2(fd) + \mathcal{O}(\gamma^3). \quad (146)$$

Taking into account Eqs. (142), (144) and (145) we have

$$\partial_\tau(fd) = -d\partial_\zeta f + \sigma\eta(p - f) - \gamma I_s(|f|^2 - 1)f + \mathcal{O}(\gamma^2), \quad (147)$$

$$\partial_{\tau\tau}^2(fd) = \partial_{\zeta\zeta}^2 f + \mathcal{O}(\gamma), \quad (148)$$

which, inserted into Eq. (146), yield

$$p = fd + \gamma[\sigma\eta(1 - d)f + (d - \gamma\sigma\eta)\partial_\zeta f] + \gamma^2[I_s(|f|^2 - 1)f + \partial_{\zeta\zeta}^2 f] + \mathcal{O}(\gamma^3). \quad (149)$$

Substituting this into Eqs. (142) and (144) we finally get the generalized complex rate equations

$$\begin{aligned} (\partial_\tau + \partial_\zeta)f &= \sigma\eta[f(d - 1)(1 - \gamma\sigma\eta) + \gamma(d - \gamma\sigma\eta)\partial_\zeta f] \\ &\quad + \gamma^2\sigma\eta[I_s(|f|^2 - 1)f + \partial_{\zeta\zeta}^2 f], \end{aligned} \quad (150)$$

$$\partial_\tau d = \gamma[1 - d + I_s(1 - |f|^2d)] - \frac{1}{2}\gamma^2 I_s \partial_\zeta |f|^2, \quad (151)$$

which are exact up to order γ^2 . In the UFL we can set $\eta = 1$ and $I_s = A - 1$, and all the parameters in the right hand sides of the rate equations become constant.

As a test of this reduced model we have determined the linear stability of the steady lasing solution ($f = 1, d = 1$) versus perturbations of the type $\delta x(\zeta, \tau) = \delta x_0(\zeta) \exp(\lambda\tau)$, with $x = f, d$, and $\delta f_0(0) = \delta f_0(\zeta_m)$, Eq. (141). Solving the characteristic polynomial perturbatively up to order γ^2 one recovers Eq. (125) in Sect. 2.3.1, as it must be. Notice finally that by making the limit $\gamma \rightarrow 0$ in Eqs. (150,151) (i.e., removing the terms multiplied by γ in the field equation and the terms multiplied by γ^2 in the inversion equation), the standard rate equations are recovered.

2.3.4 The pulse equation

The simplest multimode solution which arises from the RNGHI consists in regular pulses travelling along the cavity. If the homogeneous stationary solution is first destabilized by the N -th sidemode, N identical pulses are present simultaneously in the cavity. A semi-analytical study of the pulse solution can be already found in [31]. In 1989 Fu analyzed in detail the pulses and their stability in class-B lasers [62]. The results of Fu were obtained in the UFL. Using the rate equations (150) and (151) derived in the previous section we can not only quickly recover them, but extend them to a class-B laser outside the UFL.

We look for a solution of Eqs. (150) and (151) which travels at velocity v along the cavity. To this aim we introduce the new variable $\tau' = \tau - \zeta/v$, and we consider the following expansions

$$\begin{aligned} f &= f_0(\tau') + \gamma f_1(\tau') + \mathcal{O}(\gamma^2), & d &= 1 + \gamma I_s(\zeta) d_1(\tau') + \mathcal{O}(\gamma^2), \\ \frac{1}{v} &= 1 - \gamma \sigma \beta + \mathcal{O}(\gamma^2). \end{aligned} \quad (152)$$

We also assume that f_0 and f_1 are real and that the periodicity condition

$$x(\tau' + NT) = x(\tau'), \quad (153)$$

holds for $x = f_0, f_1, d_1$, where T is the duration of the single pulse, and N is the number of pulses circulating in the cavity. Denoting differentiation with respect to τ' by a dot, the leading order pulse equations are

$$(\eta + \beta) \dot{f}_0 - I_s \eta f_0 d_1 = 0, \quad (154)$$

$$\dot{d}_1 - 1 + f_0^2 = 0. \quad (155)$$

We can get rid of the dependence on ζ of I_s and $\eta = A/(1 + I_s)$ by averaging both sides of Eq. (154) on ζ from 0 to ζ_m . We denote this average by $\langle \dots \rangle$. Taking into account that the variation of I_s along ζ is ruled by Eq. (48), with $\chi = \Delta = 0$, we find that

$$\langle \eta \rangle = 1, \quad \langle I_s \eta \rangle = A - 1. \quad (156)$$

If we define $I_0 = f_0^2$, the pulse equations read

$$\dot{I}_0 = \frac{2(A-1)}{1+\beta} I_0 d_1, \quad (157)$$

$$\dot{d}_1 = 1 - I_0. \quad (158)$$

The parameter β can be determined by means of the solvability condition of the next order problem, which imposes that β must take one of the two values

$$\beta_{\pm} = \frac{2(A-1)}{\alpha_{\pm}^2} - 1, \quad (159)$$

where $\alpha_{\pm}(A, \mathcal{R})$ are the boundaries of the stability domain of the homogeneous solution given by Eqs. (125–126) in Sect. 2.3.1. The final form of the pulse equations is then

$$\dot{I}_0 = \alpha_{\pm}^2 I_0 d_1, \quad (160)$$

$$\dot{d}_1 = 1 - I_0. \quad (161)$$

These equations allow to calculate with a very good approximation the pulse shape in the limit $\gamma \rightarrow 0$, by-passing the problem of the very long transients associated with the full set of Maxwell–Bloch equations, and also with the generalized rate equations, in that limit. We have just to determine, for any pump A , reflectivity \mathcal{R} , and cavity length $\zeta_m = 2\pi/\tilde{\alpha}$, the correct initial conditions which give a periodic solution.

To this aim we observe that Eqs. (160–161) have a Hamiltonian structure, which can be better put in evidence with the change of variables $x = \ln I_0$, $p = d_1$ [31]. The equations for x and p read

$$\dot{x} = \alpha_{\pm}^2 p, \quad (162)$$

$$\dot{p} = 1 - e^x, \quad (163)$$

which are the equations of an anharmonic oscillator of mass α_{\pm}^{-2} subjected to the potential $V(x) = e^x - x$. A constant of motion for this system is the energy

$$H(x, p) = \alpha_{\pm}^2 \frac{p^2}{2} + V(x), \quad (164)$$

from which Eqs. (162–163) can be derived through Hamilton’s equations. The anharmonic oscillator bounces between the point x_{\min} and x_{\max} where $p = 0$. Hence, we have

$$H = V(x_{\min}) = V(x_{\max}), \quad (165)$$

which establishes a relation between x_{\min} and x_{\max} . From Eq. (164) we obtain

$$p = \frac{\sqrt{2}}{\alpha_{\pm}} \sqrt{H - V(x)}, \quad (166)$$

which can be inserted in Eq. (162) to obtain the time spent by the oscillator to move from point x_1 to point x_2

$$\tau_{12} = \frac{1}{\sqrt{2}\alpha_{\pm}} \int_{x_1}^{x_2} \frac{dx}{\sqrt{H - V(x)}}. \quad (167)$$

The period of a complete pulse is twice the time spent to go from x_{\min} to x_{\max} . For the N -pulse solution it must be equal to $2\pi/\alpha_N$, which means

$$\alpha_{\pm}(A, \mathcal{R}) = \frac{\alpha_N}{\sqrt{2}\pi} \int_{x_{\min}}^{x_{\max}} \frac{dx}{\sqrt{H - V(x)}}. \quad (168)$$

Since x_{\min} and x_{\max} are related by Eq. (165), for any given α_N and \mathcal{R} Eq. (168) allows to determine A as a function of $x_{\min} = \ln I_{\min}$ (or $x_{\max} = \ln I_{\max}$)

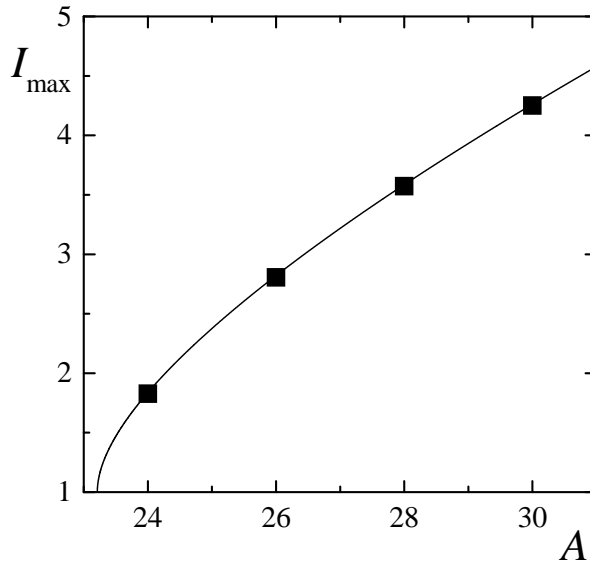


Figure 10: Maximum intensity of the 1-pulse solution according with Eqs. (165) and (168) for $\mathcal{R} = 0.7$ and $\tilde{\alpha} = 2\pi$. The bifurcation is supercritical. The squares represent the value obtained by numerical integration of the laser equations.

and then I_{\min} (or I_{\max}) as a function of A . Eq. (168) has two solutions corresponding to the two signs of α_{\pm} . It can be easily demonstrated that the integral in Eq. (168) tends to $\sqrt{2}\pi$ in the limit $x_{\min}, x_{\max} \rightarrow 0$, *i.e.* when the pulse solution reduces to the homogeneous one $I = 1$ [62]. Hence, in that limit Eq. (168) reduces to $\alpha_{\pm} = \alpha_N$. This means that the pulse solutions associated with α_+ and α_- are the multimode solutions emerging, respectively, from the upper (α_+) and lower (α_-) instability domain of the homogeneous solution. General arguments of bifurcation theory corroborated by the results of the numerical simulations indicate that only the former is stable.

The plots of $I_{\max} = I_{\max}(A)$ show that the bifurcation from the homogeneous solution to the pulse solution is supercritical or subcritical depending on whether α_N is larger or smaller than α_c . In Figs. 10 and 11 we considered a rather small value of the reflectivity, $\mathcal{R} = 0.7$. This choice of \mathcal{R} corresponds to a very bad resonator, in which the fraction of power lost per roundtrip is $(1 - \mathcal{R}^2) = 0.51$. Thus, we are very far from the UFL. For this value of \mathcal{R} the critical and minimum values of α are, respectively, $\alpha_c = 4.252$ and $\alpha_{\min} = 4.212$, and the critical pump is $A_c = 13.055$. In Fig. 10 we consider the value $\alpha_N = 2\pi$, larger than α_c , while in Fig. 11 we set $\alpha_N = 4.22$, which is intermediate between α_{\min} and α_c . The solid (dotted) lines correspond to the stable (unstable) pulse solution associated with α_+ (α_-). When the bifurcation is subcritical, the pulse solution is stable also below the instability threshold up to A_c , and in this interval it coexists

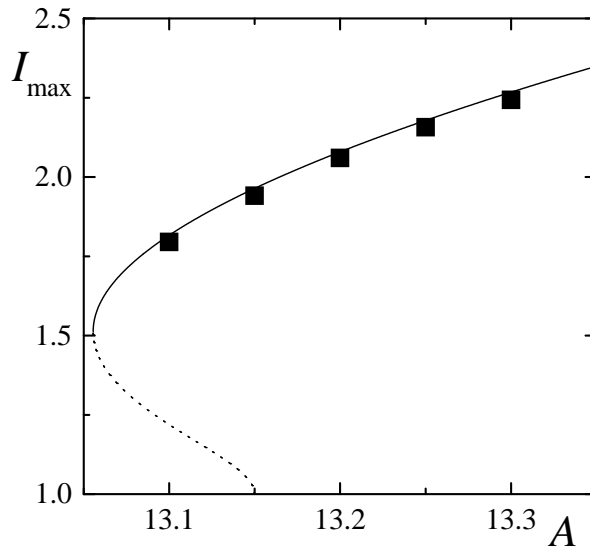


Figure 11: Same as Fig. 10 for $\tilde{\alpha} = 4.22$. Here the bifurcation is subcritical.

with the stable homogeneous solution, see Sect. 2.3.6. However, we notice that this happens only in the narrow range of values of α_N between α_{\min} and α_c .

In Figs. 10 and 11 the symbols indicate the peak intensity of the pulse obtained by the numerical integration of the dynamical equations. The agreement with the curve $I_{\max}(A)$ calculated using Eqs. (165) and (168) is very good.

The stability of the N -pulse with $N \geq 2$ was analyzed in [62] in the UFL using the Floquet method. It was found that the N -pulse solution becomes unstable beyond a certain value of I_{\max} which depends only on N . For instance $I_{\max} = 4.914$ for $N = 2$ and $I_{\max} = 2.339$ for $N = 3$. For $N = 1$ the stability analysis is more difficult and, to our knowledge, it remains an unresolved problem.

2.3.5 Numerical results

In the previous section we have illustrated a method to calculate the N -pulse multimode solution developed by the laser beyond the RNGHI threshold. In this way we can determine at once the long-term regime of the laser, skipping all the transient evolution. This is an enormous advantage from the computational point of view, because we know that the unstable eigenvalue is of order γ^2 , which means that the time scale of the transient is of order γ^{-2} .

But when the pulse solution itself destabilizes, the only way to study the laser dynamics is the numerical integration of the dynamical equations (18–20), with the boundary condition (21)⁸. These are Partial Differential Equations (PDEs)

⁸The pulsing regime has been studied numerically by few authors [31, 32, 42, 43, 46, 66]

that can be integrated using the finite difference method originally proposed by Risken and Nummedal [31]. However, the efficiency of this method is strongly limited by the fact that it imposes the constraint of equal time and space step. Since the time step is proportional to γ , in the limit of very small γ the computational time diverges, because the above mentioned constraint implies that the number of points of the spatial grid is proportional to γ^{-1} .

An alternative method consists in a modal expansion of the electric field in Fourier modes, which allows to convert the PDEs into a set of Ordinary Differential Equations (ODEs). The big advantage of ODEs is that they can be integrated using standard Runge-Kutta methods, which are easier to implement and generally run faster than the finite difference methods used for integrating PDEs.

It is commonly believed that modal expansion is convenient only in the UFL, because only in that limit the electric field can be described properly by a limited number of modes. Outside that limit, even the stationary solution requires a high number modes, because it has a nontrivial spatial dependence along the longitudinal direction [56], and the situation certainly worsens when the RNGHI sets on.

However, it was demonstrated that in class B lasers a modal expansion of the electric field is fully justified for the study of the RNGHI, even outside the UFL, *i.e.* for any mirror reflectivity [80]. This result is a simple consequence of the fact that, according to Eq. (122) derived in Section 2.3.1, the unstable modes in the RNGHI depend on ζ as

$$F_s(\zeta) \exp[-\lambda_n \zeta - \psi_n(\zeta)] , \quad (169)$$

where $\psi_n(\zeta)$ is given by Eq. (124) with $\lambda = \lambda_n$, and λ_n is a solution of the characteristic equation (123). The important point is that $\lambda_n \approx -i\alpha_n$, where α_n is the spatial frequency of the n -th mode, and $\psi_n(\zeta) \approx 0$ in two limiting cases: (i) in the UFL, and (ii) in the class-B limit $\gamma \rightarrow 0$. Then, in both limits at the leading order the unstable modes can be approximated by

$$F_s(\zeta) \exp(i\alpha_n \zeta) . \quad (170)$$

In the UFL, where $F_s = \sqrt{A - 1}$ can be assumed independent of ζ , the unstable modes immediately coincide with the empty cavity modes $\exp(i\alpha_n \zeta)$. But this is true also for class-B lasers beyond the UFL, provided the scaled electric field f defined by Eq. (137), which is equal to 1 in the stationary state, is considered in place of F . Therefore, the modal expansion can be applied to the Maxwell-Bloch equations (138–140) written in Sect. 2.3.3 for the scaled variables f , p and d and to the generalized rate equations that we derived from them. In both cases the periodic boundary condition

$$f(0, \tau) = f(\zeta_m, \tau) , \quad \zeta_m = 2\pi/\tilde{\alpha} , \quad (171)$$

and these studies have been quite superficial in most cases.

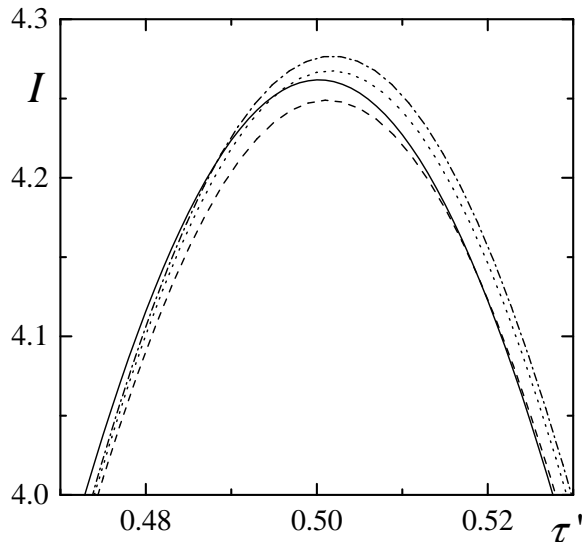


Figure 12: Enlargement of the steady pulse around the maximum for $\gamma = 0.01$. The four outputs obtained with the four different methods described in the text are compared.

allows for a modal expansion of the electric field f

$$f(\zeta, \tau) = \sum_{n=-\infty}^{+\infty} e^{i\alpha_n \zeta} f_n(\tau), \quad (172)$$

and the ODEs are simply obtained by inserting this expansion in the equation for the electric field. For the complete Maxwell-Bloch equations the equation for the generic mode amplitude f_n is

$$\frac{df_n}{d\tau} = -i\alpha_n f_n + \sigma \int_0^{\zeta_m} d\zeta \eta(\zeta) \exp(-i\alpha_n \zeta) (p - f). \quad (173)$$

The integral can be evaluated over a grid of points ζ_l , $l = 1, \dots, L$. To do that we need to know only the values of p and d in those points. Thus, we have to consider a set of ODEs for the mode amplitudes $f_n(\tau)$ and the variables $p_l(\tau) = p(\zeta_l, \tau)$ and $d_l(\tau) = d(\zeta_l, \tau)$.

For the rate equations we proceed similarly, but with two big advantages: the number of ODEs is smaller because the polarization has been adiabatically eliminated, and the stiffness of the equations has been reduced because the fast time scale associated with the polarization has disappeared.

Summarizing, we can then use three different methods to study numerically the laser equations: (i) the finite difference method applied to the full Maxwell-Bloch equations, (ii) the modal expansion technique applied to the Maxwell-Bloch equations, and (iii) the modal expansion technique applied to the rate

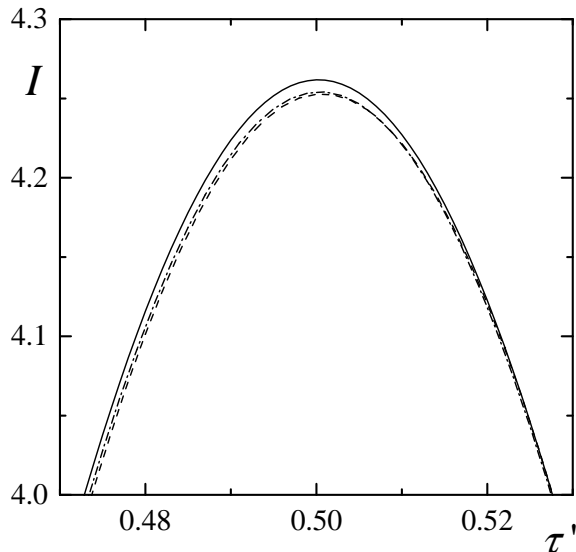


Figure 13: Same as Fig. 12 for $\gamma = 0.001$. Here only three curves are shown because the integration of the PDEs was too time consuming.

equations. Method (iii) is expected to be more efficient than method (ii), and method (ii) more efficient than method (i). On the other hand, only method (i) is applied to the full set of Maxwell-Bloch equations, while with methods (ii) and (iii) some approximations are introduced.

In Figs. 10 and 11 the symbols refer to the calculations made with method (ii), but on that scale the results of the three methods are hardly distinguishable. A better check of the correctness of the three methods and of their respective efficiency is the comparison among the shape of the calculated pulses and that of the semi-analytic pulse solution found in the previous section, which is the result to which any dynamical simulation must tend in the limit $\gamma \rightarrow 0$.

We chose to make the comparison for $\mathcal{R} = 0.7$ and $A = 30$, and we consider the $N = 1$ pulse, setting $\alpha_N = \alpha_1 = \tilde{\alpha} = 2\pi$, which implies $\sigma = 0.357$. The results of the numerical simulations are shown in Fig. 12 for $\gamma = 10^{-2}$ and in Fig. 13 for $\gamma = 10^{-3}$. In both figures we show an enlargement of the portion of the pulse around the maximum to emphasize the differences among the various integration methods. The solid lines represent the semi-analytic solution, the dotted lines the integration of the PDEs, the dashed lines the integration of the ODEs derived from the complete model, and the dotted-dashed lines the integration of the ODEs derived from the rate equations.

As expected, for the smaller value of γ the agreement between the numerical simulations and the analytic result is better. As for the computation times, for $\gamma = 0.01$ the ratios among the three methods are 5.8:1.6:1, so their efficiency is still comparable. But for $\gamma = 0.001$ the ODEs derived from the rate equations

are about 7 times faster than those derived from the complete model, and the PDEs are already too slow to converge in a reasonable time. These results demonstrate that to simulate the dynamical behavior of a fibre laser, for which $\gamma \sim 10^{-5}$, the ODEs derived from the rate equations are the only practical tool.

2.3.6 Subcriticality of the RNGH

An important issue of the RNGH that we have referred to only superficially in Sect. 2.3.4, is the subcritical or supercritical character of the bifurcation leading from singlemode to multimode emission. This issue has been considered in the past, as we detail below, within the UFL and may be important for the correct understanding of the experimental results, see Sec 4. We will here present some numerical results outside that limit, and therefore treat this question in this section.

In their second paper of 1968 [31], Risken and Nummedal already treated this question. They commented on their numerical finding that multimode emission persisted for a given pump even when the spatial frequency α was decreased below α_- , see Eq. (125), where the linear stability analysis predicts stable singlemode emission. They explicitly comment that for $\alpha < \alpha_-$ there is bistability between the singlemode and the multimode solutions.

Later on, Haken and Ohno [38, 39] obtained an equation for the critical mode and found this coexistence of solutions again. In fact they derived a condition for supercritical or subcritical bifurcation but they did not give the dependence on the wavenumber α of their result because of the excessive complexity of their equations. Lugiato *et al.* [46] derived an approximated multimode solution (from a five-mode truncation of the Maxwell–Bloch equations) that explicitly showed the bistable behavior. The question was taken up again by Fu [62] who derived the unambiguous condition in the limit of class-B lasers that we have already found in Sect. 2.3.4: The bifurcation is supercritical (subcritical) when $\alpha > \alpha_c$ ($\alpha < \alpha_c$). Finally, Carr and Erneux [64] analytically obtained the same result in a slightly different limit for class-B lasers ($\gamma_{||}/\kappa \ll 1$, which in our notation corresponds to small γ and large σ).

As stated, all these studies were carried out within the UFL. The meaning of these results is that multimode emission could be found for parameter settings for which the singlemode solution is still stable. Nevertheless, in all previous studies, the minimum instability threshold pump $r_c = 9$ for class-B lasers was found to be a lower bound for multimode emission. Outside the UFL this question has not been treated before, to the best of our knowledge. The analytical treatment has in fact been presented in Sect. 2.3.4, where we have commented on this. Here we present preliminary numerical results [92] obtained with the modal expansion technique applied to the rate equations (150,151). In Fig. 14 we represent both the linear stability multimode emission threshold and the (numerically determined) domain of existence of stable multimode emission as a function of the reflectivity of the cavity for $\alpha = \alpha_c$ ($\mathcal{R} \rightarrow 1$) = $\sqrt{12}$ and $\gamma = 0.01$. The remarkable result is that multimode emission extends well beyond the limits in reflectivity marked by the linear stability analysis, although the pump nec-

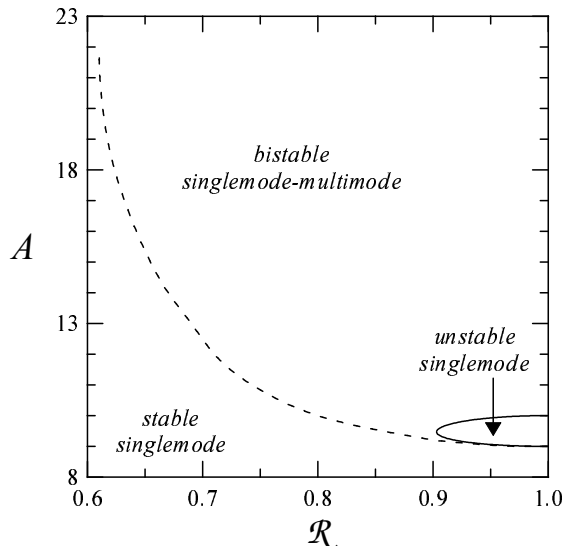


Figure 14: The dashed line indicates the limit of the domain of existence of pulsing solutions in the $\langle \mathcal{R}, A \rangle$ plane for $\alpha = \sqrt{12}$ and $\gamma = 0.01$, as obtained by the numerical integration of the rate equations model, Eqs. (150,151). The solid line is the prediction of the linear stability analysis, Eq. (125).

essary is always larger than $A_c = 9$, the value theoretically predicted in Sect. 2.3.4. This means that the domain of bistability between the singlemode and the multimode solutions is very large and, consequently, multimode pulsations could be experimentally observed for parameters for which the theory predicts singlemode emission. We shall come back to this later on when discussing the experimental observations.

3 MULTILONGITUDINAL MODE EMISSION IN INHOMOGENEOUSLY BROADENED RING LASERS

Up to now we have only considered ring lasers with a homogeneously broadened active medium. Nevertheless most lasers present some kind of inhomogeneous broadening in the gain line: In gas lasers the Maxwellian distribution of atomic velocities introduces Doppler broadening, and in solid state and fibre lasers differences in the sites of excited atoms introduce some spread in their transition frequency [11, 22, 23, 24].

From the point of view of multimode emission, inhomogeneous broadening in ring cavity lasers is of primary importance as it is well known that these

lasers easily emit in several longitudinal modes because of spectral hole burning [11, 22, 23, 24]. This mechanism for multimode emission is intuitively understood by imagining the different cavity modes, whose frequencies fall within the inhomogeneous linewidth, interacting independently with different subsets of atoms whose frequencies are quasis resonant with that of each longitudinal mode. If the different mode frequencies are well separated, as compared with the homogeneous linewidth, the above is a good picture of what actually happens in most inhomogeneously broadened ring lasers. When the frequencies of adjacent modes are moved closer together, or when their intensities grow and they undergo power broadening, some interaction between the modes may appear, mainly through saturation effects. All this has been well known for a long time and is not particularly exciting from the viewpoint of laser instabilities.

Nevertheless this image may be too naive: In the previous sections we have analyzed in detail how Rabi-splitting induced gain leads to multimode emission in homogeneously broadened lasers. Then natural questions arise immediately: How does this mechanism affect multimode emission in inhomogeneously broadened lasers? Or in other terms, how does inhomogeneous broadening affect the RNGHI? Are there two different mechanisms, namely Rabi-splitting induced gain and spectral hole burning, for multimode emission in inhomogeneously broadened lasers?

The rest of this section is organized as follows. In Sect. 3.1 we present the Maxwell-Bloch and rate equations models. Then we analyze the multimode emission threshold, first in the UFL (Sect. 3.2) and then outside this limit (Sect. 3.3). In Sect. 3.2 we pay special attention to the comparison between Maxwell-Bloch equations and rate equations.

3.1 Modelling

As in the previous sections, we consider an incoherently pumped two-level active medium of length L_m , contained in a ring cavity of length L_c , interacting with a unidirectional plane wave laser field. However, now the field interacts with an inhomogeneously broadened active medium. We model the medium by considering a Lorentzian distribution of atomic frequencies. We further assume, for the sake of simplicity, that the cavity is resonant with the center of the atomic transition frequency distribution.

3.1.1 Maxwell-Bloch equations

The Maxwell-Bloch equations describing such a laser can be easily written by generalizing Eqs. (18–20). The generalization consists in replacing the polarization appearing in the field equation Eq. (18) by the weighted sum of the polarizations corresponding to the different frequencies ω . The model equations

read [12, 53, 81, 93]

$$(\partial_\tau + \partial_\zeta) F(\zeta, \tau) = \sigma A \int_{-\infty}^{+\infty} d\omega \mathcal{L}(\omega) P, \quad (174)$$

$$\partial_\tau P(\omega, \zeta, \tau) = \gamma^{-1} [-(1 + i\omega)P + FD], \quad (175)$$

$$\partial_\tau D(\omega, \zeta, \tau) = \gamma [1 - D - \text{Re}(F^*P)], \quad (176)$$

supplemented by the boundary condition

$$F(0, \tau) = \mathcal{R}F(\zeta_m, \tau), \quad \zeta_m = 2\pi/\tilde{\alpha}. \quad (177)$$

Notice that distributed losses have been neglected ($\chi = 0$) and resonance has been assumed between the cavity and the center of the atomic frequency distribution ($\delta = 0$).

In Eqs. (174)–(176) $F(\zeta, \tau)$ is the normalized slowly varying envelope of the laser field, and $P(\omega, \zeta, \tau)$ and $D(\omega, \zeta, \tau)$ are the normalized slowly varying envelopes of the medium polarization and the population inversion, respectively, for molecules detuned by ω with respect to the cavity resonance.

Inhomogeneous broadening is accounted for by the function $\mathcal{L}(\omega)$. It represents the spectral distribution of atomic resonances, which, in order to deal with analytical expressions, is taken to be a Lorentzian distribution of width (HWHM) u

$$\mathcal{L}(\omega) = \frac{1}{\pi} \frac{u}{u^2 + \omega^2}, \quad (178)$$

where both ω and u are frequencies scaled to the homogeneous linewidth γ_\perp . With our notation the unscaled total gain linewidth (HWHM) of the medium is $\gamma_\perp(1 + u)$.

3.1.2 The uniform field limit

As demonstrated in Sect. 2.2, when the effective amplitude reflectivity \mathcal{R} is close to unity, one can apply the uniform field limit that consists in replacing the field Eq. (174) by

$$(\partial_\tau + \partial_\zeta) F(\zeta, \tau) = \sigma \left[-F + A \int_{-\infty}^{+\infty} d\omega \mathcal{L}(\omega) P \right], \quad (179)$$

complemented with the new boundary condition $F(0, \tau) = F(\zeta_m, \tau)$.

3.1.3 Standard rate equations (uniform field limit)

Class-B lasers (those for which $\gamma_\perp \gg \gamma_\parallel, \kappa$, i.e., $\gamma, \sigma \ll 1$), use to be described with rate equations, which are obtained after the adiabatic elimination of the medium polarization in the Maxwell–Bloch equations. These rate equations are generally assumed to be appropriate for describing multimode emission due to spectral hole burning [11]. As we shall later compare the predictions of the full set of Maxwell–Bloch equations with those of the simpler rate equations, we

give here this simpler model, whose detailed derivation can be found in [11, 94]. After expanding the field as

$$F(\zeta, \tau) = \sum_{n=-N}^{+N} \sqrt{I_n} e^{i\phi_n} \exp[i\alpha_n(\zeta - \tau)] \quad (180)$$

with $\alpha_n = n\alpha$, expanding the medium polarization in a similar way and adiabatically eliminating the polarization, one is left with the standard rate equations

$$\frac{dI_n}{d\tau} = 2\sigma I_n \left[A \int_{-\infty}^{\infty} d\omega \frac{\mathcal{L}(\omega)D}{1 + (\omega - \alpha_n)^2} - 1 \right], \quad (181)$$

$$\frac{\partial D}{\partial \tau} = \gamma - \gamma D \left[1 + \sum_n \frac{I_n}{1 + (\omega - \alpha_n)^2} \right]. \quad (182)$$

The phases can be calculated through

$$\frac{d\phi_n}{d\tau} = -\sigma A \int_{-\infty}^{\infty} d\omega \frac{\mathcal{L}(\omega)D(\omega - \alpha_n)}{1 + (\omega - \alpha_n)^2}. \quad (183)$$

In these equations, the integer index n denotes the n -th longitudinal mode with respect to the central resonant mode ($n = 0$). As we show below, the rate equations description is not appropriate for too long cavities, where *long* may actually be quite short.

3.2 Multimode emission in the uniform field limit

The stability properties of the uniform field limit were treated first by Mandel [53, 54] (see also [12]), who showed that in the limit $u \rightarrow \infty$, the multimode emission threshold is just above the lasing threshold. The general case has been treated at depth in [81], and the reader is referred to that publication for full details.

Eqs. (175,176,179) have two stationary solutions: The laser-off solution ($F = 0$, $P = 0$, $D = 1$), and the monomode solution, for which the intensity of the lasing mode, $I_0 = F^2$, can be written as $A = \sqrt{1 + I_0} (\sqrt{1 + I_0} + u)$. The threshold for lasing emission is found by taking $I_0 = 0$ in this expression, and thus it occurs at a pump $A = A_0 \equiv 1 + u$. Then, by defining the normalized pump parameter $r = A/A_0$, the lasing solution reads

$$r = \frac{R(R + u)}{1 + u}, \quad (184)$$

$$R = \sqrt{1 + I_0}, \quad (185)$$

or

$$I_0 = r(1 + u) - 1 + \frac{1}{2}u \left(u - \sqrt{u^2 + 4r(1 + u)} \right), \quad (186)$$

which for $u = 0$ gives $I_0 = r - 1$. At threshold, $R = r = 1$.

3.2.1 Two estimates of the multimode emission threshold

Let us assume momentarily the following naïve approach: Assume that the threshold for amplification of a detuned mode is not affected by the already existing resonant lasing mode. This assumption will be reasonably accurate whenever (i) the inhomogeneous width u is large, because in that case the intensity I_0 of the resonant mode at threshold for multimode emission will be small, and (ii) when the frequency Ω of the detuned mode is (sufficiently) larger than the normalized homogeneous width γ^{-1} (which is a measure of the width of the spectral hole), *i.e.*, for large α .

In [81] we showed that under these assumptions the emission threshold for a sidemode of spatial frequency α can be estimated to be given by

$$r_{\text{thr}}(\alpha) = 1 + \left(\frac{\gamma\alpha}{\gamma\sigma + 1 + u} \right)^2 \rightarrow r_{\text{thr},B}(\alpha) = 1 + \left(\frac{\gamma\alpha}{1 + u} \right)^2, \quad (187)$$

where the limit corresponds to class-B lasers ($\gamma \ll 1$). Thus multimode emission occurs, in this simple approach, for $r > r_{\text{thr}}$. The term $\gamma\alpha/(1 + u)$ represents the sidemode frequency offset divided by the sum of the cavity linewidth and the total gain linewidth. One can think of Eq. (187) as the multimode emission threshold when spectral hole burning is the only relevant mechanism for multimode emission and there is not any interaction between modes.

A second, more accurate, estimate for the multimode emission threshold for class-B lasers is obtained from the rate equations model, Eqs. (181, 182). The derivation can be found in Chapter 4 of Khanin's book [11] (see also [81]). It reads

$$0 = p(R) + \gamma^2\alpha^2, \quad (188)$$

$$p(R) = R^2(1 - u) + R(1 - u)(u + 2) + (u + 1)^2, \quad (189)$$

when the cross relaxation coefficient γ_{CR} is set equal to zero in Khanin's equations [11]. By using Eq. (184), the above equation can be rewritten as

$$r_{\text{rate}} = r_{\text{thr},B}(\alpha) + \frac{2R(R + 1)}{(1 + u)^2}, \quad (190)$$

with $r_{\text{thr},B}(\alpha)$ given by Eq. (187) and R given by Eq. (185), the monomode solution being unstable for $r > r_{\text{rate}}$. We see that $r_{\text{rate}} \geq r_{\text{thr},B}(\alpha)$, *i.e.*, the instability threshold given by Eq. (190) is always larger than the one predicted by Eq. (187), which was admittedly valid for $\alpha \gg 1$. Both boundaries tend to coincide in the limits of validity of Eq. (187), *i.e.*, $u \gg 1$. This is perfectly reasonable as Eq. (190) contains one more ingredient with respect to Eq. (187), namely the saturation of the sideband gain due to the resonant mode, which explains why it gives a larger value for the instability threshold.

Notice that Eq. (190) predicts that there will be no multimode emission unless $u > 1$, *i.e.*, it fails in predicting multimode emission due to Rabi-splitting induced gain (RNGHI). This is entirely normal as the rate equations do not

contain information about the atomic coherence, i.e., about the medium polarization dynamics, which is the responsible for the RNGHI as we have seen in the previous section. On the other hand, the limitation $u > 1$ does not appear in the naïve approach of Eq. (187). Then the physical picture is the following: For $u < 1$, even if the threshold for emission for more than one mode is crossed, the nonlinear competition between the different cavity modes enforces that only one of them lases. This is an example of “the winner takes all” competition and is the common picture of multimode dynamics — which we know to be false because of the RNGHI.

The existence of a minimum instability threshold in the limit $\alpha \rightarrow 0$ predicted by the rate equations, Eq. (190), is quite unphysical, because it would mean that the closer are the sidemodes to the central mode, the lower is its instability threshold. This erroneous result is a consequence of the approximations introduced in the derivation of the rate equations, and it disappears when the stability analysis of the homogenous solution is performed using the full set of Maxwell–Bloch equations. As will be shown below, the complete model predicts that, for a given pump value, there is always a minimum value of the frequency spacing α below which there is no instability because the gain of the sidemodes is saturated by the strong central mode.

3.2.2 Multimode emission threshold

The multimode emission threshold is rigorously obtained by performing a linear stability analysis of the single–mode solution Eq. (184). The analytical expressions obtained are cumbersome and it is not trivial to extract analytical information. We refer the interested reader to [81] where several limits of interest are treated explicitly. Here we shall make a resume of the results concerning class–B lasers. Two limits of interest can be treated explicitly for class–B lasers: The short and long cavity limits, *i.e.*, the limits $\alpha \gg 1$ and $\alpha = \mathcal{O}(1)$ or smaller.

For short cavities, $\alpha \gg 1$, the instability threshold turns out to be given by Eq. (190). This amounts to saying that for short cavities the rate equations approach is valid for deriving the multimode emission threshold.

For long cavities, $\alpha = \mathcal{O}(1)$, an approximate expression for the multimode emission threshold can be derived. It is given by

$$\begin{aligned} \mathcal{P} &= 0, \\ \mathcal{P} &= p(R)\alpha^4 - 3(R^2 - 1)[(R + u + 1)^2 - Ru]\alpha^2 \\ &\quad + R(R^2 - 1)(R + 1)^2(R + u)(u + 2), \end{aligned} \tag{191}$$

with $p(R)$ given by Eq. (189). The monomode solution is unstable for $\mathcal{P} < 0$. Before comparing this multimode emission threshold with that predicted by the rate equations, we show the influence of the inhomogeneous broadening on the multimode instability threshold. In Fig. 15 we represent the multimode emission threshold predicted by Eq. (191) for several values of u in the $\langle r, \alpha \rangle$ plane. Notice the enormous quantitative effect that the inhomogeneous broadening has on the instability threshold. In fact, it can be shown analytically [81] that the

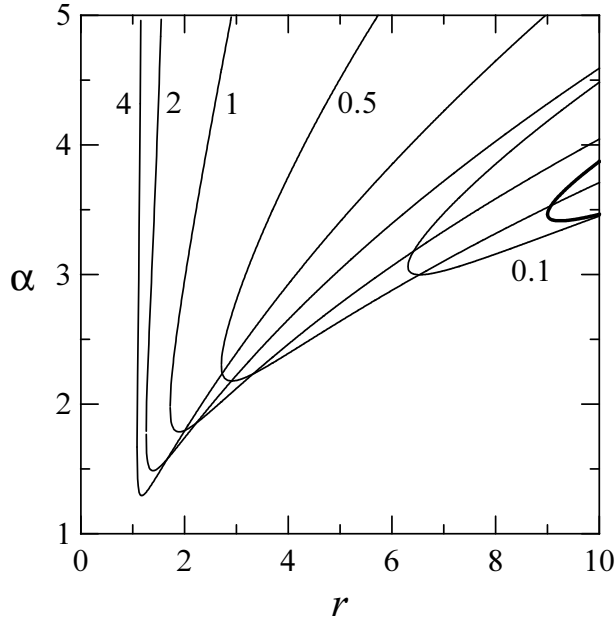


Figure 15: Multimode emission threshold in the $\langle r, \alpha \rangle$ plane for the values of the inhomogeneous to homogeneous linewidth ratio, u , marked in the figure. The thick line corresponds to the homogeneous limit $u = 0$.

critical point $\langle r_c, \alpha_c \rangle$, that for which r is minimum at the instability threshold, varies as

$$r_c = 9 - 36u + \mathcal{O}(u^2), \quad (192)$$

$$\alpha_c^2 = 12 - 33.75u + \mathcal{O}(u^2), \quad (193)$$

for $u \ll 1$, and as

$$r_c = 1 + 32/(17u^2) + \mathcal{O}(u^{-3}), \quad (194)$$

$$\alpha_c^2 = 8/3 + 80/(17u^2) + \mathcal{O}(u^{-3}). \quad (195)$$

for $u \gg 1$.

In Fig. 16 the thresholds predicted by Eq. (188) (dashed line) and Eq. (191) (full line) are represented in the $\langle r, \alpha \rangle$ plane for $u = 4$. The exact instability threshold (diamonds) as obtained by numerically solving Eq. (22) in [81], is also shown. Several conclusions can be extracted from this figure.

(i) There is a single instability threshold, *i.e.*, there are not two mechanisms for multimode emission (spectral hole burning and RNGHI) but a single mechanism;

(ii) The asymptotic expressions Eqs. (188) and (191) compare perfectly well with the exact result in their respective domains of validity: The threshold

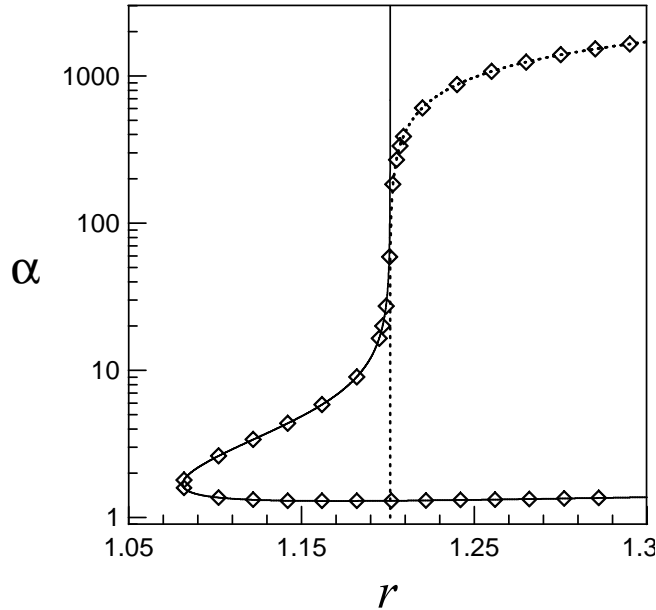


Figure 16: Multimode emission threshold for $u = 4$. The solid (dashed) lines have been obtained from Eqs. (191) and (188), respectively. The diamonds correspond to the exact stability analysis of the Maxwell–Bloch equations, Eq. (22) in Ref. [81], and have been calculated for $\gamma = 10^{-3}$ and $\sigma = 0.1$.

predicted by the rate equations becomes invalid for small α (long cavity) while the approximate expression Eq. (191) becomes invalid for large α (short cavity);

(iii) The unphysical instability predicted for small α by the rate equations result is removed, and there is a minimum value of α below which there is no instability; and

(iv) there is a domain of intermediate cavity lengths where the two analytic expressions connect.

The last item allows to determine which is the value of the cavity length beyond which the rate equations approach is no more valid. By analyzing Eqs. (188) and (191) one obtains that the distance between the two functions is minimum for $\alpha \sim 2\gamma^{-1/2}$ when $u \geq 2$. This leads to a “coherence length” estimate

$$L_{\text{coh}} = \frac{\pi C}{\gamma_{\perp}} \left(\frac{\gamma_{\perp}}{\gamma_{\parallel}} \right)^{1/4}, \quad (196)$$

for lasers with a significant inhomogeneous broadening ($u \geq 2$).

Then, for cavities larger than L_{coh} , atomic coherence effects (*i.e.*, Rabi-splitting induced gain) are important for the determination of the multimode emission threshold while they are irrelevant for shorter cavities. For example,

for CO₂ lasers $L_{\text{coh}} \approx 100$ m, for 632.8 nm HeNe lasers $L_{\text{coh}} \approx 20$ m, for Er³⁺-doped fibre lasers $L_{\text{coh}} \approx 5$ cm, and for Nd-glass lasers $L_{\text{coh}} \approx 3$ mm. Thus, the necessity of using the full Maxwell–Bloch description of the laser in order to describe multimode emission depends strongly on the particular laser system under consideration: It is necessary for Nd-glass and Er³⁺-doped fibre lasers and unnecessary for CO₂ and HeNe lasers.

Let us remark that the expression for L_{coh} gives a good estimate for the critical length for values of $u \geq 2$; for smaller values of u , L_{coh} decrease, tending to 0 for $u \rightarrow 1$, so that the necessity of considering coherent effects is still more important in this limit.

The above shows that Rabi-induced sidemode gain (RNGHI) is far from being a negligible mechanism for multimode emission in inhomogeneously broadened ring lasers. Quite to the contrary, it is an essential ingredient for those lasers with cavity lengths larger than L_{coh} or even shorter if the ratio of inhomogeneous to homogeneous linewidth is small.

3.2.3 Dynamics beyond the multimode emission threshold

The numerical integration of the inhomogeneously broadened model is far from being a simple task, especially for class-B lasers. In fact, this task has been carried out very recently for the first time in [94]. For the sake of illustration, let us comment that some of the calculations we comment below implied a running time of more than one month on a R12000 Silicon Graphics processor. This illustrates the enormous difficulties of making numerical simulations for class-B laser parameters, due to the stiffness of the equations in this limit.

There were previous attempts, during the eighties, by Brunner et al. [95, 96] of numerically studying multimode emission in inhomogeneously broadened lasers. But the model they used was that of a standing-wave cavity and the third-order Lamb theory approximation was assumed. As this approximation does not contain atomic coherence effects, their results did not give information about the RNGHI mechanism in standing-wave lasers.

In [94], the Maxwell–Bloch Eqs. (175,176,179) and the rate equations model Eqs. (181,182) were numerically integrated for fixed pump ($r = 5$), inhomogeneous broadening ($u = 2$) and spatial frequency (equal to the homogeneous linewidth), and three different values of γ (10^{-1} , 10^{-2} , and 10^{-3}). As we change the value of γ over three orders of magnitude, we change the Rabi frequency of the field. In doing so, the behavior makes the transition from that predicted by the rate-equations model (for smaller γ) to that in which Rabi-induced gain effects are expected to be important (for larger γ). The main finding in [94] consists in the confirmation of the conclusions extracted from the stability properties: Rate equations describe properly the multimode dynamics only for short cavities, that is, under conditions for which the free spectral range is large as compared to the Rabi frequency of the intracavity field. In this limit rate equations and Maxwell–Bloch equations provide the same results for the mode intensities at steady state, and no phase locking is found even in the Maxwell–Bloch equation, where all relevant information about the phase dynamics is

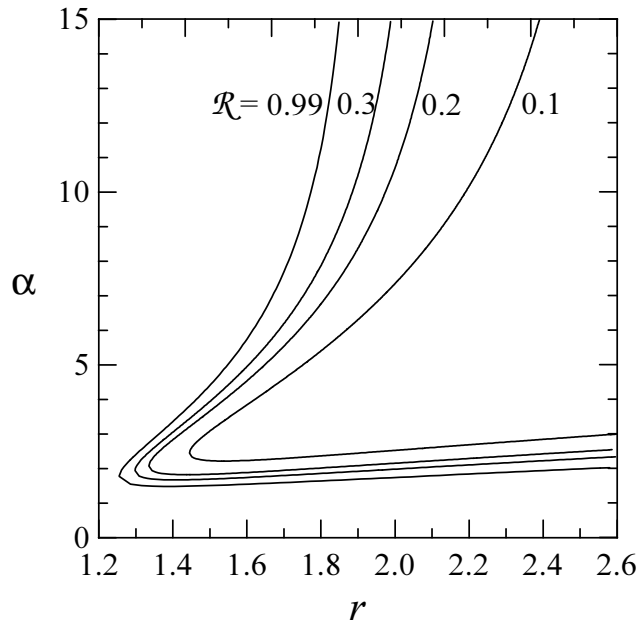


Figure 17: Multimode emission threshold in the $\langle r, \alpha \rangle$ plane for $u = 2$ and the values of the reflectivity marked in the figure as obtained from Eq. (36) in [93].

preserved (remember that mode-locking cannot be described by the rate equations model as modal phases do not enter in the dynamics of mode intensities and population inversion, see Eqs. (181–183)). Then, for short cavities the use of rate equations is perfectly legitimate.

This is no longer true for longer cavities, where the inhomogeneously broadened laser behaves like a homogeneously broadened one, with a multimode dynamics which presents all the features of the classical RNGHI: The number of excited modes is larger than expected from linear stability considerations and phases spontaneously lock, giving rise to regular pulses in the total intensity. We refer the reader to [94] for full details.

3.3 Multimode emission outside the uniform field limit

Outside the uniform field limit, *i.e.*, for arbitrary values of the amplitude reflectivity \mathcal{R} the analytical expressions for the instability threshold are much more involved than in the uniform field limit previously analyzed. For class-B lasers the problem has been treated in detail in [93], and the interested reader is referred to that paper for full details. Here we shall stress some important points.

As it happens in the homogeneously broadened model, a decrease in the value of \mathcal{R} leads to an increase of the multimode emission threshold. This can

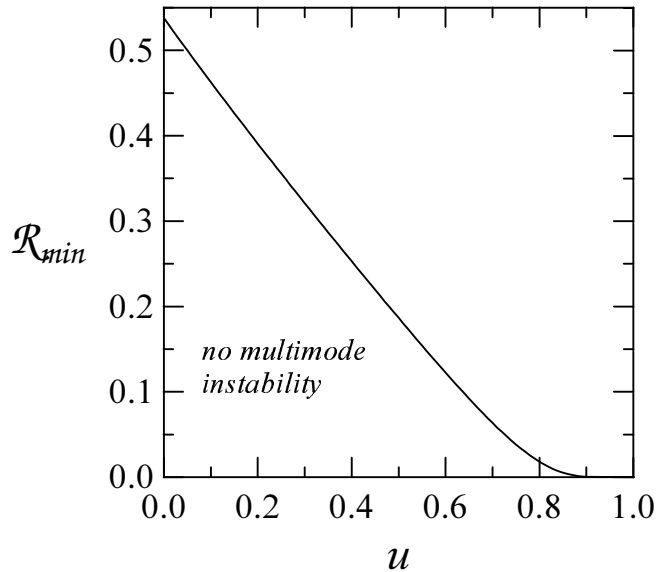


Figure 18: Minimum value of the reflectivity for the multimode instability to exist, \mathcal{R}_{\min} , as a function of the inhomogeneous to homogeneous linewidth ratio.

be seen in Fig. 17 where the multimode instability threshold is shown, as usual, in the $\langle r, \alpha \rangle$ plane for $u = 2$ and several values of the amplitude reflectivity \mathcal{R} . For $\mathcal{R} = 0.99$, the instability threshold is very close to that predicted by the homogeneously broadened model (Eq. (191)), and decreasing values of \mathcal{R} increase the instability threshold as expected. What is unexpected is that multimode emission exists for values of \mathcal{R} as low as 0.1. This is unexpected because we showed analytically in Sect. 2.3.1 that in homogeneously broadened lasers, the decrease of \mathcal{R} leads to the disappearance of the multimode instability when $\mathcal{R} < \mathcal{R}_{\min} \simeq 0.538$.

Fortunately, \mathcal{R}_{\min} can be analytically determined even outside the uniform field limit (see [93]). It is given by $\mathcal{D}(\mathcal{R}, u) = 0$ with

$$\mathcal{D}(\mathcal{R}, u) = 9 - 4 \left[1 - \frac{u(u+1)}{2} \right] \frac{1 + \mathcal{R}^2}{1 - \mathcal{R}^2} |\ln \mathcal{R}^2|, \quad (197)$$

which reduces to Eq. (126) for $u = 0$ ⁹.

In Fig. 18 \mathcal{R}_{\min} is shown as a function of u . Notice that the limitation on the value of \mathcal{R} for the existence of multimode emission disappears at $u = 1$ (although in practical terms it disappears for $u > 0.9$ as \mathcal{R}_{\min} decreases exponentially as $u \rightarrow 1$). Thus the multimode instability does not have any limitation in cavity losses when inhomogeneous broadening is about the same

⁹Notice that Eq. (197) corrects a typographic error in Eq. (46) of [93].

as the inhomogeneous width or larger. This marks an important difference with the case of homogeneous broadening. The fact that this qualitative change appears at $u = 1$ can be related to the fact that the rate equations model predicts the multimode instability only for $u > 1$. This result suggests that for $u > 1$ spectral hole burning makes multimode emission possible when the Rabi-induced gain mechanism could not do it by itself (*i.e.*, there is no more a \mathcal{R}_{\min} , which is a characteristic of the RNGHI), while for $u < 1$, \mathcal{R}_{\min} exists (although its values decreases for increasing u). This suggests that spectral hole burning plays a less important role in this limit.

This result is particularly relevant from the experimental point of view: An increase of the cavity losses eventually leads to the impossibility of multimode emission when $u < 0.9$ (*i.e.*, for homogeneously broadened lasers or lasers with small inhomogeneous broadening), but this does not happen for lasers with enough inhomogeneous broadening at $u > 0.9$.

3.3.1 Effect of distributed losses in three-level and four-level lasers

In Sect. 2.3.2, where homogeneous broadening was considered, it was shown that distributed losses have quantitative importance for the determination of the multimode emission threshold for three- and four-level lasers, although it was not really important for two-level lasers as far as distributed losses have reasonable values, roughly below 10dB. The reason lies in the way how losses enter in the transformation of the pump parameter for applying the results of the two-level theory to three- and four-level lasers.

For inhomogeneously broadened lasers the same argument holds, and distributed losses must be taken into account when calculating the multimode instability threshold for three- and four-level lasers. Performing the linear stability analysis with inhomogeneous broadening and distributed losses outside the uniform field limit is a very heavy task that does not provide any analytical insight. Rather than going to that trouble, it suffices at least in the case of not too large distributed losses to use the results of the linear stability analysis outside the uniform field limit without distributed losses, and introduce them when calculating the transformation of the pump parameter, as already explained in Sect. 2.3.2. This is the way we calculated the instability threshold presented in [89] and reproduced in the following section (cf. Fig. 21 below). For more details, see Ref. 24 in [89].

4 ON EXPERIMENTAL STUDIES OF THE MULTIMODE INSTABILITY IN EDFL's

In this section we describe experimental observations that contribute to the discussion of multimode laser instabilities. We already discussed in Sect. 1 that experimental research on the RNGHI has been limited to the dye laser [44, 45] and that the observed multimode emission was explained as being caused by the band structure of the lasing levels [47, 48, 49], not a manifestation of the

RNGHI. Prior to Refs. [71, 72] no other experimental work on the subject has appeared. The reason is probably that the constraints imposed on the cavity length by Eqs. (93) and (100) have discouraged experimentalists: According to Eq. (100), cavity lengths need to be enormously long (in some cases several orders of magnitude longer than standard values), while at the same time there is the requirement of a very large instability to lasing threshold ratio (the “factor-of-nine”) [2]. By now it is known, however, that the “factor-of-nine” is irrelevant if the active medium is better modelled as a three-level laser medium. Moreover, for such lasers Eq. (100) does not constitute a hard limit, as for cavity lengths well below this value instabilities occur at accessible pump values. This makes it much more likely that the RNGHI becomes observable in some lasers.

By this reasoning, Er-doped fiber lasers are rendered the most promising candidate for a clear observation of the RNGHI: these are three-level lasers, and their cavities can be made very long. We will therefore concentrate on this laser type.

Many laser applications require monochromatic operation, and therefore several researchers attempted to operate Er-doped fiber laser in single mode operation. However, after many failures and a few partial successes, this is now considered as notoriously difficult. Where it was attempted, researchers chose one of these strategies: (i) increase the cavity’s effective free spectral range beyond the gain bandwidth (see, e.g., [97]), or (ii) reduce the gain bandwidth below the free spectral range by insertion of filters with very narrow bandwidth (see, e.g. [98]). None of these approaches led to a full success. For example, in a publication subsequent to [98] it is reported that single mode operation became impossible to maintain above a certain pump level [99]. The reason for this behavior was not further investigated.

The pragmatic conclusion is that EDFL’s obviously have a natural tendency to operate on several modes simultaneously. The small free spectral range caused by the necessarily long resonator contributes to the difficulty, but by itself cannot explain the underlying reason.

4.1 A first dedicated approach

Probably the first experimental study of fundamental causes for the instability of an EDFL was presented in [71]. The authors made a distinction between relaxation oscillation and self mode locking, and investigated the latter. They used a resonator consisting of a WDM coupler to bring in the pump light, and an output coupler to steer fully 90% of the power out. A polarization-insensitive optical isolator enforced unidirectional operation. An Er-doped active fiber provided gain; alternatively either a 15 m length at low dopant concentration (300 ppm), or a 0.8 m length at high concentration (≈ 5000 ppm) was used. Allowing for some extra length of component pigtailed, this brought the resonator’s free spectral range to about 10 MHz or 70 MHz, respectively.

The laser output was directed through another isolator and then monitored either by a fast photodiode hooked up to a fast oscilloscope or an RF spectrum analyzer, or by a background-free autocorrelator. No stable cw emission was ob-

served. For the longer cavity it was reported that self-modelocking produced a train of pulses with a repetition rate given by the resonator’s free spectral range. An occasional presence of satellite pulses at intermediate times was mentioned. The pulses were reported to have a temporal width (FWHM) of a few ns. Inspection with the autocorrelator was performed to check for substructure. The autocorrelator could monitor a time window of 50 ps, and within this window no substructure was found. For the shorter cavity, a modulation of the output power at the free spectral range was also observed. However, it did not take the form of pulses but rather had a nearly sinusoidal shape. This is plausible because for a larger free spectral range, fewer modes will fall into the bandwidth of the gain.

When the pump power was varied near lasing threshold, in the shorter cavity the instability was seen whenever there was lasing, while in the longer cavity a small interval of single-mode operation seemed to exist just above lasing threshold.

4.2 The follow-up

In a subsequent study [72], basically the same group of authors replaced the polarization-insensitive isolator with a polarizing isolator. They also added polarization controllers to the cavity. Two output couplers branching out 95% or 50% were used alternatively. The active fiber was again of the low Er concentration type, and was 13 m long. The cavity free spectral range was thus near 10 MHz. Again, self mode locking at the cavity free spectral range was observed; pulses had a duration of 1.74...3.00 ns. The RF spectrum contained ≈ 250 beat notes, indicative of a similar number of oscillating modes.

In this experiment there was a combination of fiber birefringence plus polarizing elements in the cavity. This raises the issue whether mode locking due to Nonlinear Polarization Rotation (NPR) might have occurred. The authors argue that NPR can be ruled out for the following reasons: (i) In the previous setup, there definitely was no picosecond structure, and when the polarizing isolator was introduced, the pulse shape was not modified. This suggests — somewhat indirectly — that the polarizing action is not responsible. The authors further noted that (ii) at times intermediate to the pulses there was a constant background of random signal, possibly satellite pulses of some kind, and that NPR would likely suppress such structure. However, random groups of pulses are routinely seen in NPR lasers. Finally, (iii) power levels in the fiber were deemed insufficient for NPR, in particular since a wide core fiber was used. NPR requires remarkably little power, however, and at the powers stated, NPR cannot be ruled out entirely. However, the authors kindly inform us that the instability also existed just above threshold, and in that case NPR is indeed highly unlikely to occur.

There remains an unresolved discrepancy about the measured spectral shape of the pulses which is reported to be Gaussian and, for 2 ns pulses, must have been 0,001 nm wide. The optical spectrum analyzer reportedly used for this measurement, however, has a specified spectral resolution of 0,05 nm.

One of the most prominent features of RNGHI, namely its threshold-like onset, was not addressed in the experiment of [72]. The publication provides a comment that the experiments took place far above lasing thresholds, but that instability persisted down to at least a less-than-tenfold threshold power. As the authors kindly inform us, the instability was seen immediately above lasing threshold. From this information one must conclude that the matter deserves more clarification before anything is definitely proven.

4.3 A systematic assessments of thresholds

In subsequent work, an Er-doped fiber ring laser specifically designed for observation of instabilities was set up by some of the present authors. As a starting point a standard configuration was chosen, see Fig. 19. The cavity contained 8.2 m of active fiber (585 ppm Er dopant level) in a 22 m long ring (the remainder consisted of standard single mode fiber). Pump light came from a 100 mW, 980 nm laser diode; it was launched into the ring by a WDM coupler. Light coupled out by this WDM coupler, and also from an additional 95/5 coupler, was used to monitor the system simultaneously by a fast photodiode and an optical spectrum analyzer. An optical isolator ensured unidirectional operation, and a moderately narrow bandpass filter gently restricted the bandwidth available for lasing to about 1 nm. As a unique feature, variable loss was inserted into the cavity. To this end either an amplitude modulator or a tight fiber coil with well-defined radius was employed. High variable loss served to bring out the onset of instability more clearly. Great effort was made to characterize the exact amount of loss for each setting: all components (localized losses) including splices etc. were tested individually, and the distributed loss in the Er fiber was determined. Finally, as a cross-check the total loss was calculated from the operational laser's output power vs. pump power relation. For more detail see [89]. Just above lasing threshold this laser indeed operated in a single longitudinal mode. As the pump power was increased, modulations of the output power appeared at frequencies which were integer multiples of the cavity round trip frequency (9 MHz) without exception. Obviously these were beat notes between different longitudinal modes.

These beat notes, however, were neither steady in amplitude, nor in frequency: The frequencies involved hopped rapidly and apparently at random all across the range up to several GHz, and during much of the time in between there was no beat at all. After the insertion of the bandpass filter already mentioned above, the frequency hopping range was limited to hundreds of MHz and thus more manageable. Still, the beats remained unsteady. A typical beat note episode lasted on the order of tens of milliseconds to a few seconds. The temporal profile of the beat note was almost always very nearly sinusoidal, indicative of a beat between only two resonator modes. In the presence of the high loss intentionally introduced here, the laser could not be pumped very far above threshold, so that it may be not too surprising that there was just dual-mode, but no multimode operation.

We wish to point out that for this experiment nonlinear polarization rotation

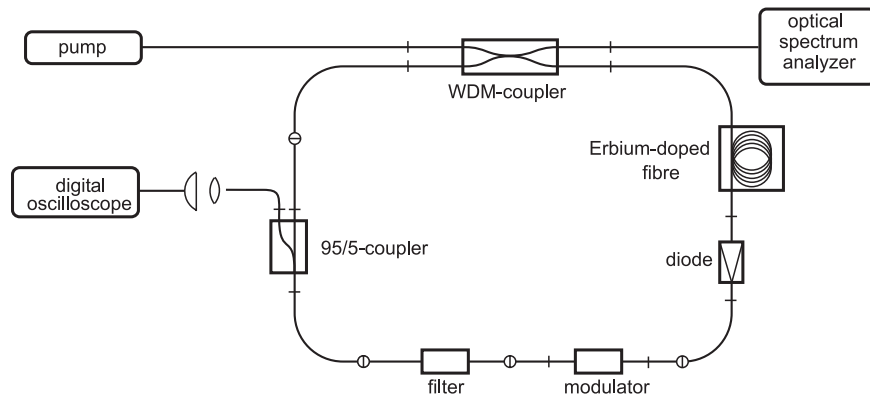


Figure 19: Experimental setup. The modulator serves to introduce well-defined loss; it can take the form of either an electro-optic modulator or a tightly wound fiber coil. For further detail see text.

(NPR) [100] can be safely ruled out. Polarization-dependent losses, on which NPR hinges, were carefully avoided.

Given a random phenomenon, statistical means were employed to characterize it. Time series of the instantaneous power were recorded which — in view of the typical timescales — were chosen to be several seconds long. Unfortunately, adequate sampling to correctly assess all up to the highest frequencies would have required data rates of GB/s and file sizes of about 10 GB per shot; that is just not feasible. To keep data files at manageable size, undersampling at 20 000 samples per second was chosen. While this way information about the actual beat frequency is lost, all episodes of mode beating longer than $100 \mu\text{s}$ still can be detected from the time series. Shorter episodes seemed not to occur anyway. Occasional occurrences of relaxation oscillation were easily identified in the file by their very different amplitude, and were discarded. The fraction of time during which valid mode beats were detected served as the measure of instability M .

The data-taking procedure consisted in setting a particular loss value, then incrementing the pump power in small steps, and determining M at each step. (At the same time, as described above, the total power was recorded to help assess the loss value). Next, the loss was incremented, and the procedure was repeated until the accessible range of loss values was exhausted. After an evaluation of these extensive data, the following conclusions are reached: The laser power data in Fig. 20 show the universally known threshold behavior: the power is close to zero below threshold, but not exactly so due to fluorescence. Above threshold the power makes a good fit to a straight line by which the slope efficiency is defined. The measure of instability, on the other hand, strictly remains at zero up to some point above the laser threshold. Beyond that point, M sharply sets on to nonzero values, and continues to rise as the pump power

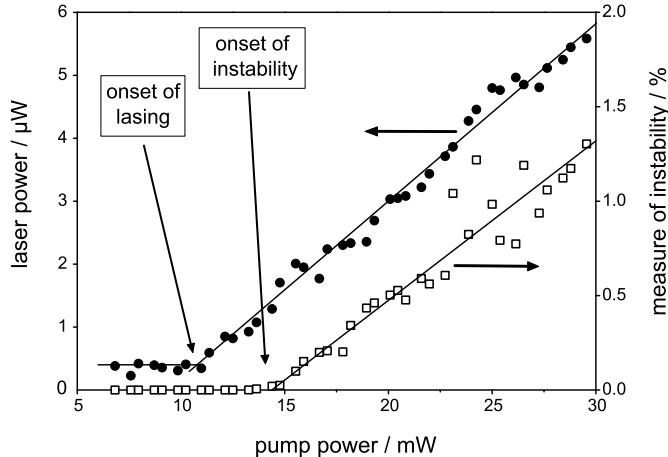


Figure 20: Laser power (filled circles) and measure of instability (open squares) as a function of pump power.

is raised further. This is clear evidence that the instability has a well-defined, sharp onset, a fact which had not previously been demonstrated experimentally.

In the next step both the lasing threshold and the instability onset are taken from data as in Fig. 20. Fig. 21 reveals that the ratio of both values P_{inst}/P_0 (where P_{inst} and P_0 denote the pump power at the instability and lasing thresholds, respectively) does indeed scale with loss. At low loss, $P_{\text{inst}}/P_0 \approx 1$. Under typical operating conditions of Er fiber lasers, losses would be even lower, and experimenters would be unable to tell apart both onsets. For larger loss, however, P_{inst}/P_0 increases up to about 1.5. The intentionally high loss of this experiment pays off nicely here: Both onsets are clearly distinguishable, and the interval of single mode operation in between is clearly identifiable. This constitutes a considerable progress over previous work.

However, we must emphasize an important fact regarding the range of loss values used in that experiment. We showed in Sect. 2.3.1 that in a homogeneously broadened gain medium \mathcal{R}_{min} describes a maximum value of loss beyond which there exists no instability at all. \mathcal{R}_{min} as defined in Eq. 129 corresponds to 4.5 dB of localized loss in the experiment [89], but Fig. 21 clearly shows that instability persists at much higher loss.

To resolve this discrepancy, we reconsider the structure of the Er gain line. In Sect. 3.3 we showed that in the case of an inhomogeneous contribution to the line as expressed by $u \neq 0$, \mathcal{R}_{min} goes to zero (see the discussion of Eq. 197 and Fig. 18); hence the corresponding maximum loss diverges. It is difficult to make precise statements about the value of u for the fiber used in the

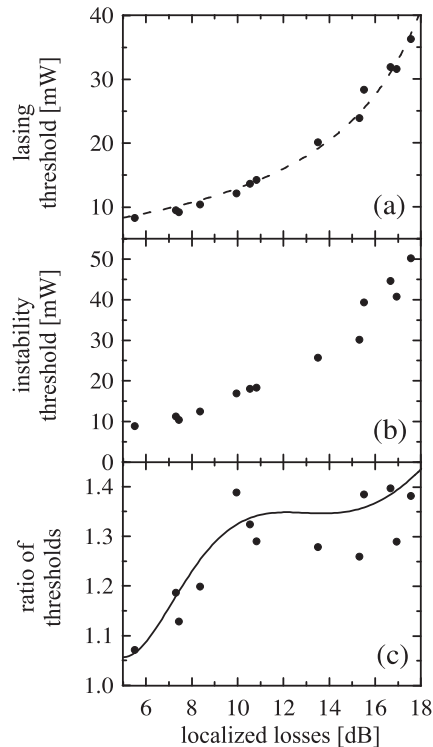


Figure 21: Influence of localized cavity loss. Shown are (a) the laser threshold, (b) the instability onset, and (c) the ratio of both. The dashed line in (a) is a fit with theory (see [89] for more detail); while the line in (c) only serves to guide the eye.

experiment in [89], but a choice of $u = 2$ is reasonable. For this value, Fig. 22 shows the theoretically expected threshold ratio as a function of localized cavity loss (the calculation takes distributed losses into account, see [89] for details). Evidently, the disagreement with experimental data is reduced dramatically. While quantitatively r is systematically predicted too high, in particular at the highest loss values, at least the discrepancy about the *existence* of an instability onset is resolved.

Finally we need to address a caveat about the interpretation of the experimentally observed instability onset. As was discussed in Secs. 2.3.4, 2.3.6, the possibility exists that the instability threshold is either a supercritical or a subcritical bifurcation. Based on experimental data alone, a decision between these possibilities cannot be made. Consider a subcritical bifurcation, which would in all likelihood imply a range of bistability between the single-mode and the multimode solution (at least this is the case in the homogeneously broadened case, see Fig. 18). The observed intermittent behavior would make some sense

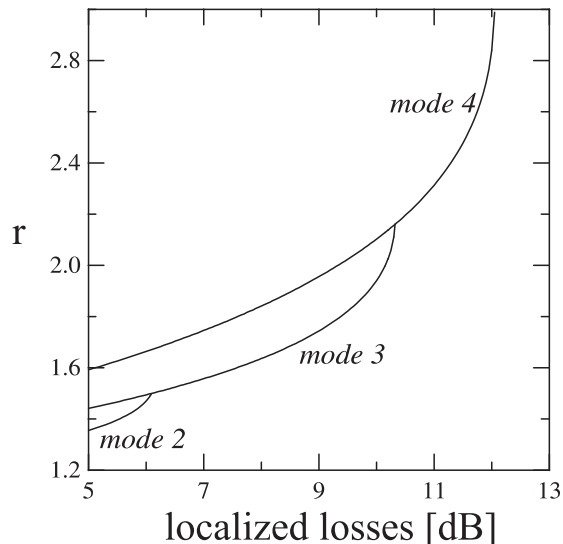


Figure 22: Ratio of instability onset to lasing threshold, as predicted by a three-level laser model with inhomogeneous broadening at $u = 2$. Different modes become unstable at different points; the labels refer them to the central lasing mode. For the instability onset, always the lowest line counts.

in that case: The experimentally determined instability onset would then be the lower limit point of the unstable branch, and the bifurcation proper was never reached due to limited available pump power. In fact, not even the point of "Maxwell's construction" (where both branches are occupied for equal amounts of time on average) was reached. Even if unlimited pump power had been available, it is not at all clear whether a final conclusion about the nature of the bifurcation could have been reached, because a sizeable increase of the pump power eventually brings on other processes like Brillouin scattering, thermal effects, etc., which further complicate the issue. We must therefore leave this question open for now.

Let us finally remark that, in contrast to [72], *multimode* operation and pulsing was never observed in [89]: there was only dual-mode operation and sinusoidal modulation. Also, there were only intermittent, not steady, beat notes between modes. Surely, this must have to do with the fact that the laser was intentionally made lossy so that it could never be pumped very much above its first threshold. Whether there are still other factors involved (codopants of the fiber, etc.) must remain unresolved at this point.

5 CONCLUSION AND OUTLOOK

We have introduced the different models required for the study of the RNGHI. In particular, we have treated the applicability of the two-level laser model to three- and four-level lasers and, importantly, the rigorous derivation of the uniform field limit. We have then revised the basics of the RNGHI, and we have reviewed our continued work on the subject over recent years. This research was motivated by the suggestion by Lugiato and coworkers in 1997 [72] that the pulsations exhibited by a unidirectional EDFL could be a manifestation of this elusive phenomenon.

At long last, the threshold-like onset of the multimode instability in an EDFL was demonstrated in [89]. Data show a qualitative and, with appropriate corrections, even semi-quantitative agreement to theoretical expectations. Nevertheless, data do not represent a clear-cut textbook rendition of the RNGHI, but only an approximation. Therefore the bottom line of our combined theoretical and experimental research is this: The processes observed in EDFLs very likely constitute a manifestation of the RNGHI, but it is a manifestation in a 'dressed' way. Inhomogeneous broadening, distributed losses, and the three-level structure of erbium ions take their imprint on the instability. Moreover, it is very likely that noise plays a central role in the 'intermittent' appearance of multimode emission.

Theories are very often neater and much more elegant than real-world experiments. The closest thing to Lorenz-type laser chaos that was ever found experimentally suffered from complications that are absent from the model, as we commented in Sect. 1. In a similar way, the experiment in [89] presents the closest thing to RNGHI that has been found to date. In any case, we do not have any doubt that the experimental observations are a clear manifestation of the resonant Rabi instability, i.e., that Rabi sideband gain is the responsible for the observed instability.

Another remarkable result of our research is that the RNGH mechanism is essential for understanding the multimode emission threshold in inhomogeneously broadened lasers, even for relatively short values of the laser cavity depending on the active medium. This fact suggests that RNGHI could be important for correctly understanding mode-locking in lasers with an accessible coherence length (see Eq. (196) and the subsequent discussion).

Finally we would like to remark that there are open questions from both the theoretical and the experimental sides. On the one hand, the observed intermittent pulsations needs to be theoretically explained, and it must be determined up to what extent subcriticality and noise could explain them, or whether other phenomena we have not yet considered (such as dispersion or fiber nonlinearity [67, 13]) need to be taken into account. On the other hand, experimental research in other laser types, as NdDFLs or Nd:YAG lasers, would help to understand how the RNGH mechanism affects real lasers.

We gratefully acknowledge J.L. Font, F. Fontana, L.A. Lugiato, M. Lenz, E.M. Pessina, J. Redondo, F. Silva, and J.F. Urchueguía for continued discussions on the subject along the recent years. We thank J.L. Font for carrying

out the numerical calculations represented in Fig. 14 [92]. This work has been supported by the Spanish Ministerio de Ciencia y Tecnología and European Union FEDER (Fonds Européen de Développement Régional) through Project PB2002-04369-C04-01, and by Deutsche Forschungsgemeinschaft

References

- [1] T. H. Maiman, *Stimulated Optical Emission in Fluorescent Solids. II. Spectroscopy and Stimulated Emission in Ruby*, Phys. Rev. **123**, 1151–1157 (1961).
- [2] C. O. Weiss and R. Vilaseca, *Dynamics of Lasers*, (VCH Verlagsgesellschaft, Weinheim, 1991).
- [3] F. T. Arecchi and R. G. Harrison, *Selected papers on Optical Chaos*, (SPIE Milestones Series, vol. MS75, 1993).
- [4] F. Prati, M. Brambilla, and L. A. Lugiato, *Pattern Formation in Lasers*, Riv. Nuovo Cimento **17**, 1–85 (1994).
- [5] N. B. Abraham, L. A. Lugiato, and L. M. Narducci (Eds.) J. Opt. Soc. Am. B **2** (issue 1) Special Issue on Instabilities in Active Optical Media (1985).
- [6] D. K. Bandy, A. N. Oraevsky, and J. R. Tredicce (Eds.) J. Opt. Soc. Am. B **2** (issue 5) Special Issue on Nonlinear Dynamics of Lasers (1988).
- [7] R.W. Boyd, M.G. Raymer, and L.M. Narducci (Eds.), *Optical Instabilities* (Cambridge University Press, Cambridge, 1986).
- [8] F. T. Arecchi, R. G. Harrison (Eds.), *Instabilities and Chaos in Quantum Optics*, (Springer, Berlin, 1987).
- [9] L. M. Narducci, N. B. Abraham, *Laser Physics and Laser Instabilities*, (World Scientific, Singapore, 1988).
- [10] N. B. Abraham, P. Mandel, L. M. Narducci, *Dynamical Instabilities and Pulsations in Lasers*, in: Progress in Optics XXV, p. 1-190, Elsevier Science B.V., Amsterdam (1988).
- [11] Ya. I. Khanin, *Principles of Laser Dynamics*, (Elsevier Science B.V., Amsterdam, 1995).
- [12] P. Mandel, *Theoretical Problems in Cavity Nonlinear Optics*, (Cambridge University Press, Cambridge, 1997).
- [13] G.H.M. Tartwijk and G.P. Agrawal, *Laser Instabilities: a Modern Perspective*, Prog. Quant. Electron. **22**, 43–122 (1998)

- [14] L. A. Lugiato and L. M. Narducci, *Single-mode and multimode instabilities in lasers and related optical systems*, Phys. Rev. A **32**, 1576–1587 (1985).
- [15] H. Haken, *Analogy between higher instabilities in fluids and lasers*, Phys. Lett. **53A**, 77–78 (1975).
- [16] E. Lorenz, *Deterministic nonperiodic flow*, J. Atmos. Sci. **20**, 130–141 (1963).
- [17] C. O. Weiss and W. Klische, *On observability of Lorenz instability in lasers*, Opt. Commun. **51**, 47–48 (1984).
- [18] C. O. Weiss and J. Brock, *Evidence for Lorenz-Type Chaos in a laser*, Phys. Rev. Lett. **57**, 2804–2806 (1986).
- [19] C. O. Weiss, N. B. Abraham, and U. Hübner, *Homoclinic and Heteroclinic Chaos in a Single-Mode Laser*, Phys. Rev. Lett. **61**, 1587–1590 (1988).
- [20] C. O. Weiss, R. Vilaseca, N. B. Abraham, R. Corbalán, E. Roldán, G. J. de Valcárcel, J. Pujol, U. Hübner, and D. Y. Tang, *Models, Predictions, and Experimental Measurements of a Far-Infrared NH₃ Laser Dynamics and Comparisons with the Lorenz-Haken Model*, Appl. Phys. B **61**, 223–242 (1995).
- [21] E. Roldán, G. J. de Valcárcel, R. Vilaseca, R. Corbalán, V. J. Martínez, and R. Gilmore, *The Dynamics of Optically-Pumped Molecular Lasers. On its Relation with the Lorenz-Haken Model*, Quantum and Semiclassical Optics **9**, R1–35 (1997).
- [22] G.H.C. New, *The generation of ultrashort laser pulses*, Rep. Prog. Phys. **46**, 877–971 (1983).
- [23] A. E. Siegman, *Lasers*, (Oxford University Press, UK, 1986).
- [24] O. Svelto, *Principles of Lasers*, (Plenum Press, New York, 1989).
- [25] C. L. Tang, H. Statz, and G. deMars, *Spectral output and spiking behavior of solid-state lasers*, J. Appl. Phys. **34**, 2289–2295 (1963).
- [26] K. Otsuka, *Multimode Laser Dynamics* Prog. in Quantum Electron. **23**, 97–129 (1999).
- [27] P. Mandel, *Global Rate Equation Description of a Laser*, Eur. Phys. J. D **8**, 431–442 (2000).
- [28] T. Hill, M. W. Hamilton, D. Pieroux, and P. Mandel, *Intensity Coherence of a Multimode Nd-doped Yttrium Aluminium Garnet Laser*, Phys. Rev. A **66**, 063803 (2002).
- [29] H. Risken and K. Nummedal, *Instability of off resonance mode in lasers*, Phys. Lett. **26A**, 275–276 (1968).

- [30] R. Graham and H. Haken, *Quantum theory of light propagation in a fluctuating laser-active medium*, Z. Phys. **213**, 420–450 (1968).
- [31] H. Risken and K. Nummedal, *Self-pulsing in laser*, J. Appl. Phys. **39**, 4662–4672 (1968).
- [32] K. Ikeda, K. Otsuka, and K. Matsumoto, *Maxwell–Bloch turbulence*, Prog. Theor. Phys. Suppl. **99**, 295–324 (1989).
- [33] R. Graham, *Onset of self-pulsing in lasers and the Lorenz model*, Phys. Lett. **58A**, 440–442 (1976).
- [34] C.-Z. Ning and H. Haken, *Detuned lasers and the complex Lorenz equations: Subcritical and supercritical Hopf bifurcations*, Phys. Rev. A **41**, 3826–3837 (1990).
- [35] A.C. Fowler, J.D. Gibbon, and M.J. McGuinness, *The complex Lorenz equations*, Physica D **4**, 139–163 (1982).
- [36] N. D. Milovski, *On the stability of a single-frequency travelling-wave laser*, Phys. Lett. **33A**, 492–493 (1970).
- [37] C. E. Halford, *Modifications of the theoretical model for a self-pulsing ring laser*, J. Appl. Phys. **44**, 5644–5646 (1973).
- [38] H. Haken and H. Ohno, *Theory of ultra-short laser pulses*, Opt. Commun. **16**, 205–208 (1976).
- [39] H. Ohno and H. Haken, *Transient ultra-short laser pulses*, Phys. Lett. **59A**, 261–263 (1976).
- [40] H. Haken and H. Ohno, *Onset of ultrashort laser pulses: first or second order phase transition?*, Opt. Commun. **26**, 117–118 (1978).
- [41] P. R. Gerber and M. Büttiker, *Stability Domain of Coherent Laser Waves*, Z. Phys. **33B**, 219–222 (1979).
- [42] M. Mayr, H. Risken, and H. D. Vollmer, *Periodic and chaotic breathing of pulses in a ringlaser*, Opt. Commun. **36**, 480–482 (1981).
- [43] J. Zorell, *Self-pulsing in lasers with detuning*, Opt. Commun. **38**, 127–130 (1981).
- [44] L. W. Hillman, J. Krasinski, R. W. Boyd, and C. R. Stroud Jr., *Observation of Higher Order Dynamical States of a Homogeneously Broadened Laser* Phys. Rev. Lett. **52**, 1605–1608 (1984).
- [45] L. W. Hillman, J. Krasinski, K. Koch, and C. R. Stroud Jr., *Dynamics of homogeneously broadened lasers: higher-order bichromatic states of operation*, J. Opt. Soc. Am. B **2**, 211–217 (1985).

- [46] L. A. Lugiato, L. M. Narducci, E. V. Eschenazi, D. K. Bandy, and N. B. Abraham, *Multimode instabilities in a homogeneously broadened ring laser*, Phys. Rev. A **32**, 1563–1575 (1985).
- [47] H. Fu and H. Haken, *Semiclassical Dye Lasers Equations and the Unidirectional Single-Frequency Operation*, Phys. Rev. A **36**, 4802–4817 (1987).
- [48] H. Fu and H. Haken, *A band model for dye laser and the low threshold of the second instability*, Opt. Commun. **64**, 454–456 (1987).
- [49] H. Fu and H. Haken, *Semiclassical Theory of Dye Lasers: The Single-Frequency and Multifrequency Steady States of Operation*, J. Opt. Soc. Am. **5**, 899–908 (1988).
- [50] B. Segard and B. Macke, *Self-Pulsing in Intrinsic Optical Bistability with Two-Level Molecules*, Phys. Rev. Lett. **60**, 412–415 (1988).
- [51] B. Segard, B. Macke, L. A. Lugiato, F. Prati, and M. Brambilla, *Multimode Instability in Optical Bistability*, Phys. Rev. A **39**, 703–722 (1989).
- [52] R. Bonifacio and L. A. Lugiato, *Instabilities for a coherently driven absorber in a ring cavity*, Lett. Nuovo Cimento **21**, 510–516 (1978).
- [53] P. Mandel, *On the stability of a multimode inhomogeneously broadened ring laser*, Opt. Commun. **53**, 249–253 (1985).
- [54] P. Mandel, *Unstable modes of an inhomogeneously broadened multimode ring laser*, in Ref. [7], pp.262–264.
- [55] H. Risken, *Single- and multimode instabilities in lasers*, in Ref.[7], pp.20–33.
- [56] L. A. Lugiato, L. M. Narducci, D. K. Bandy, and J. R. Tredicce, *Single-mode approximation in laser physics: A critique and a proposed improvement*, Phys. Rev. A **33**, 1109 (1986).
- [57] L.M. Narducci, J.R. Tredicce, L.A. Lugiato, N.B. Abraham, and D.K. Bandy, *Mode-mode competition and unstable behaviour in a homogeneously broadened ring laser*, Phys. Rev. A **33**, 1842–1854 (1986).
- [58] L. A. Lugiato, L. M. Narducci, and M. F. Squicciarini, *Exact linear stability analysis of the plane-wave Maxwell-Bloch equations for a ring lasers*, Phys. Rev. A **34**, 3101–3108 (1986).
- [59] J.N. Elgin and J.B. Molina-Garza, *Traveling-wave solutions of the Maxwell-Bloch equations*, Phys. Rev. A **35**, 3986–3988 (1987).
- [60] C. R. Doering, J. N. Elgin, J. D. Gibbon, and D.D. Holm, *Finite dimensionality in the laser equations in the good cavity limit*, Phys. Lett. **129A**, 310–316 (1988).

- [61] P. Constantin, C. Foias, and J. D. Gibbon, *Finite-dimensional attractor for the laser equations*, Nonlinearity **2**, 241–269 (1989).
- [62] H. Fu, *Analytic self-pulsing solutions and their instabilities in a homogeneously broadened laser*, Phys. Rev. A **40**, 1868–1891 (1989).
- [63] H. Fu and H. Haken, *Self-pulsing in a band model for dye lasers*, Phys. Rev. A **42**, 4151–4163 (1990).
- [64] T. W. Carr and T. Erneux, *Hopf bifurcation of the class-B multimode laser*, Phys. Rev. A **50**, 724–731 (1994).
- [65] T. W. Carr and T. Erneux, *Understanding the bifurcation to traveling waves in a class-B laser using a degenerate Ginzburg-Landau equation*, Phys. Rev. A **50**, 4219–4227 (1994).
- [66] D. Casini, G. D’Alessandro, and A. Politi, *Soft turbulence in multimode lasers*, Phys. Rev. A **55**, 751–760 (1997).
- [67] G.H.M. Tartwijk and G.P. Agrawal, *Maxwell–Bloch dynamics and modulational instabilities in fiber lasers and amplifiers*, J. Opt. Soc. Am. **14**, 2618–2627 (1997).
- [68] J. Jahanpanah and R. Loudon, *Theory of laser–amplifier linear gain*, Phys. Rev. A **56**, 2255–2266 (1997).
- [69] M. B. Pande and S. Dutta Gupta, *cw instability and steady-state pulse in a ring laser with intracavity parametric amplification*, Phys. Rev. A **46**, 7260–7269 (1992).
- [70] F. Castelli, L. A. Lugiato and R. Pirovano, *Rabi resonance in frequency conversion by four-wave mixing in lasers and its connection with the multimode laser instability*, Phys. Rev. A **49**, 4031–4037 (1994).
- [71] F. Fontana, M. Begotti, E. M. Pessina, and L. A. Lugiato, *Maxwell–Bloch modelocking instabilities in erbium-doped fibre lasers*, Opt. Commun. **114**, 89–94 (1995).
- [72] E. M. Pessina, G. Bonfrate, F. Fontana, and L. A. Lugiato, *Experimental observation of the Risken–Nummedal–Graham–Haken multimode laser instability*, Phys. Rev. A **56**, 4086–4093 (1997).
- [73] Q. L. Williams, J. Garcia–Ojalvo, and R. Roy, *Fast intracavity polarization dynamics of an erbium-doped fibre ring laser: inclusion of stochastic effects*, Phys. Rev. A **55**, 2376–2386 (1997).
- [74] E. Roldán, *Very low instability threshold in a three-level laser model with incoherent optical pumping*, Opt. Commun. **143**, 235–240 (1997).

- [75] E. Roldán and G. J. de Valcárcel, *On the observability of the Risken-Nummedal-Graham-Haken multimode instability in Erbium-doped fibre lasers*, *Europhys. Lett.* **43**, 255–260 (1998).
- [76] E. Desurvire, *Erbium Doped Fiber Amplifiers* (Wiley, New York, 1994).
- [77] E. M. Pessina, F. Prati, J. Redondo, E. Roldán, and G. J. de Valcárcel, *Multimode instability in ring fibre lasers*, *Phys. Rev. A* **60**, 2517–2528 (1999).
- [78] E. Roldán, G. J. de Valcárcel, and F. Mitschke, *Role of Field Losses on the Risken-Nummedal-Graham-Haken Instability*, *Appl. Phys. B* **76**, 741–748 (2003).
- [79] E. Roldán, G. J. de Valcárcel, J. F. Urchueguía, and J. M. Guerra, *Observability of the Risken-Nummedal-Graham-Haken Instability in Nd:YAG Lasers*, *J. Opt. Soc. Am. B* **20**, 816–824 (2003).
- [80] G. J. de Valcárcel, E. Roldán, and F. Prati, *Modal expansions in lasers outside the uniform field limit*, *J. Opt. Soc. Am. B* **20**, 825–830 (2003).
- [81] E. Roldán, G. J. de Valcárcel, F. Silva, and F. Prati, *Multimode emission in inhomogeneously-broadened ring lasers*, *J. Opt. Soc. Am. B* **18**, 1601–1611 (2001).
- [82] L. A. Lugiato and M. Milani, *Disappearance of laser instabilities in a Gaussian cavity mode*, *Opt. Commun.* **46**, 57–60 (1983).
- [83] S. Stuut and M. Sargent III, *Effects of Gaussian-beam averaging on phase conjugation and beat-frequency spectroscopy*, *J. Opt. Soc. Am. B* **1**, 95–101 (1984).
- [84] L. A. Lugiato and M. Milani, *Effects of Gaussian-beam averaging on laser instabilities*, *J. Opt. Soc. Am. B* **2**, 15–17 (1985).
- [85] C. P. Smith and R. Dykstra, *Lorenz-like chaos in a Gaussian mode laser with radially dependent gain*, *Opt. Commun.* **117**, 107–110 (1995).
- [86] J. F. Urchueguía, G. J. de Valcárcel, and E. Roldán, *Laser instabilities in a Gaussian cavity mode with Gaussian pump profile*, *J. Opt. Soc. Am. B* **15**, 1512–1520 (1998).
- [87] J. F. Urchueguía, G. J. de Valcárcel, E. Roldán, and F. Prati, *Transverse effects in ring fibre laser multimode instabilities*, *Phys. Rev. A* **62**, 041801(R) (2000).
- [88] T. Voigt, M. O. Lenz, and F. Mitschke, *Risken-Nummedal-Graham-Haken instability finally confirmed experimentally*, in *International Seminar on Novel Trends in Nonlinear Laser Spectroscopy and High-Precision Measurements in Optics*, S. N. Bagaev, V. N. Zadkov, and S. M. Arakelian eds., *Proc. SPIE* **4429**, 112–115 (2001).

- [89] T. Voigt, M. Lenz, F. Mitschke, E. Roldán, and G. J. de Valcárcel, *Experimental Investigation of Risken-Nummedal-Graham-Haken laser instability in ring fibre lasers*, Appl. Phys. B **79**, 175–184 (2004).
- [90] G. J. de Valcárcel, E. Roldán, and F. Prati, *Risken-Nummedal-Graham-Haken Instability in Class-B Lasers*, Opt. Commun. **163**, 5–8 (1999).
- [91] G. J. de Valcárcel, E. Roldán, and F. Prati, *Generalized Rate Equations for Multimode Lasers*, Opt. Commun. **216**, 203–207 (2003).
- [92] J. L. Font, R. Vilaseca, F. Prati, and E. Roldán, *Coexistence of single-mode and multi-longitudinal mode emission in the ring laser model*, in preparation.
- [93] E. Roldán and G. J. de Valcárcel, *Multimode instability in inhomogeneously broadened class B ring lasers: beyond the uniform field limit*, Phys. Rev. A **64**, 053805 (2001).
- [94] F. Prati, E. M. Pessina, E. Roldán, and G. J. de Valcárcel, *Coherent effects in the multimode dynamics of inhomogeneously broadened ring lasers*, Opt. Commun. **237**, 189–199 (2004).
- [95] W. Brunner, R. Fischer, and H. Paul, *Regular and chaotic behavior of multimode lasers*, Journ. Opt. Soc. Am. B **2**, 202–209 (1985).
- [96] W. Brunner, R. Fischer, and H. Paul, *Time evolution of the total electric field strength in multimode lasers*, Journ. Opt. Soc. Am. B **5**, 1139–1143 (1988).
- [97] J.L. Zhang, C.Y. Yue, G.W. Schinn, W.R.L. Clements, and J.W.Y. Lit, *Stable Single-Mode Compound-Ring Erbium-Doped Fiber Laser*, Journ. Lightw. Techn. **14**, 104–109 (1996).
- [98] M. J. Guy, J. R. Taylor, and R. Kashyap, *Single-frequency erbium fibre ring laser with intracavity phase-shifted Bragg grating narrowband filter*, Electron. Lett. **31**, 1924–1925 (1995).
- [99] D. I. Chang, M.J. Guy, S.V. Chernikov, J.R. Taylor, and H.J. Kong, *Single-frequency erbium fibre laser using the twisted-mode technique*, Electron. Lett. **32**, 1786–1787 (1996).
- [100] K. Tamura, H. A. Haus, and E. P. Ippen, *Self-starting additive pulse mode-locked erbium fiber ring laser*, Electron. Lett. **28**, 2226–2228 (1992).